

Highlights

The Reliability of Remotely Piloted Aircraft System Performance under Communication Loss and Latency Uncertainties

Yutian Pang, Andrew Paul Kendall, John-Paul Clarke

- We present mathematical formulations for the key metrics of Required Communication Performance (RCP).
- We introduce communicability, a novel metric that integrates transaction time, availability, and continuity within the RCP concept.
- Communication signal availability and latency parameters are incorporated into the flight simulation model of remotely piloted high-performance aircraft.
- Through Monte Carlo simulations, we derive the mission success surface envelop for the waypoint navigation task.
- We discover the performance decay behavior under availability and latency variabilities, and highlight the flight control limitations.

The Reliability of Remotely Piloted Aircraft System Performance under Communication Loss and Latency Uncertainties

Yutian Pang^{a,*}, Andrew Paul Kendall^a, John-Paul Clarke^a

^a*Department of Aerospace Engineering and Engineering Mechanics, The University of Texas at Austin, Austin, 78712, TX, USA*

Abstract

Mission-critical use of highly maneuverable Remotely Piloted Aircraft Systems (RPAS) requires a thorough understanding of the reliability of their communication systems. Investigations into system-level performance under stochastic aviation communication conditions are critical for estimating mission success rates and assessing the risks associated with integrating RPAS into existing airspace, ensuring overall aviation safety. This study aims to quantify the impact of communication latency and complete signal loss on the mission completion performance of a highly maneuverable RPAS. The mission is defined as a static waypoint tracking task in three-dimensional airspace. We start with examining and deriving mathematical formulations of key reliability metrics of Required Communication Performance (RCP). These stochastic factors are then embedded into flight control simulations (i.e., communication availability and latency) to examine the system behavior. Lastly, we generate mission success rate and mission completion time envelopes through extensive multiprocessing Monte Carlo simulations through high-performance computing. We discover a drastic deterioration in flight performance while latency or availability erodes the stability margin. In addition, we propose a new reliability metric, namely *communicability*, which integrates three key RCP metrics and helps understanding the maximum tolerable latency to flight control. The procedure and results obtained from this research inform engineers designing RPAS with better trade-off

*Corresponding author.

Email address: yutian.pang@austin.utexas.edu (Yutian Pang)

between communication capability and flight control performance. Future works includes exploring alternative flight simulators (i.e., nonlinear dynamic inversion) with other missions (i.e., dynamic waypoint following), or develop delay-compensated optimal controls. The analysis on stability margin is also desired for theoretical verification. The code used in this research can be found from this [LINK](#).

Keywords: Remotely Piloted Aircraft System, Required Communication Performance, Latency and Availability, Flight Simulations, Mission Success Envelop

1. Introduction

The Remotely Piloted Aircraft System (RPAS) stands for the end-to-end system that an unmanned Remotely Piloted Aircraft (RPA) is piloted from a Remote Pilot Station (RPS) by a Remote Pilot (RP). Such systems can carry cameras, sensors, communications equipment, or other payloads to perform specific tasks. Although RPAS have been used for reconnaissance and information gathering of military operations since the 1950s (i.e., High-Altitude Long Endurance unmanned aerial vehicle) (Ma'Sum et al., 2013; Chaturvedi et al., 2019), their future role has expanded considerably to the integration of RPAS into existing civilian airspace due to the gradual maturity of aerospace autonomy capabilities (Kephart and Braasch, 2010). The growing interest in RPAS stems from the versatility and operational advantages. RPAS can undertake missions in hazardous environments without placing aircrews at physical risk, thus reducing the threat to fatalities. They are also invaluable in tasks such as real-time surveillance (Iscold et al., 2010; Thammawichai et al., 2017), search and rescue (Scherer et al., 2015), and environmental monitoring (Asadzadeh et al., 2022). The ability of RPAS to remain airborne for extended periods while providing constant updates and imagery makes them an increasingly important tool for both the official and the private sector (Abeyratne and Abeyratne, 2019).

Air Traffic Management (ATM) serves as the backbone of safe and efficient flight operations within the active field of research on RPAS. ATM consists of three major functions (air traffic services, airspace management, and air traffic flow management) to ensure safe and efficient travel of aircraft within the given section of airspace (ICAO, 2006), by integrating human, software and hardware supported by communications, navigation, surveil-

lance (CNS) capabilities. Air traffic services provides services to support the daily aeronautical operations such as collision avoidance, conflict resolution, and maintain aeronautical separation minima via timely information provision (ICAO AMCP WG-C1/WP8, 2011). In recent years, emerging aviation concept such as Advanced Air Mobility (AAM), is pushing the boundaries of ATM adaptation even further. Research institutes and government agencies such as the Federal Aviation Administration (FAA), National Aeronautics and Space Administration (NASA), and the European Union Aviation Safety Agency (EASA) are leading the research effort on Advanced Air Mobility (AAM) (Goyal and Cohen, 2022; Johnson and Silva, 2022). AAM pushes air transportation to the new stage by integrating physical and digital infrastructures to efficiently move the people and cargo in the airspace, with multi-rotor vertical or short takeoff and landing aircraft ideally being electrical (eVTOL/STOL). Urban Air Mobility (UAM) is viewed as the subset of AAM where the operation are mostly at urban scenarios (MITRE Engenuity, 2023). The Urban Mobility Concept of Operation defines the AAM operates above the AAM corridors at 400 feet above ground level (AGL), and cruises between 1,500 and 4,000 AGL at the speed between 50 knots and 140 knots. Besides normal data and voice communication requirements in ATM, video streams communication is the desired function for, (a) real-time monitoring of passenger cabins; (b) command and control (C2) link of pilot video; (c) passenger entertainments (FAA, 2023). To address the increased demand for AAM/UAM operations in the urban scenario, the communication system that can works smartly becomes vital to maintain a proper workload for the controller maintaining safety and efficiency in the performance-based airspace.

However, this expanding role for RPAS comes with significant challenges to the community, particularly regarding the safe and seamless integration into the existing Air Traffic Management (ATM) system. One needs to ensure that RPAS can safely share the airspace without causing disruptions to manned aircraft. This requires the establishment of airworthiness standards and verification techniques that do not impose undue burdens on air traffic services. The lack of the standard regulations of integrating remotely piloted aircraft systems (RPAS) into existing airspace has been identified as a major challenge (Organization, 2017; Serafino et al., 2019). The integration of RPAS has been outline by the Federal Aviation Administration (FAA) (Huerta, 2013) and Single European Sky ATM Research (SESAR) joint undertaking (SESAR-JU, 2019), as well as the International Civil Avi-

ation Organization (ICAO). The long-term objective is to ensure all RPAS are regulated as routine civil operations (Teutsch and Petersen, 2022). Under this big picture, the safety guarantee of RPAS system reliability remains a challenge, along with detect and avoid system verification, and human factor satisfactory. The command and control (C2) link performance on communication latency, availability, and continuity can be evaluated in real-time, while latency and availability are reported to be sufficient for communication link performance evaluation (Serafino et al., 2019).

Researchers have been working on studying the reliability of safety-critical sub-systems in aviation (Pettit et al., 2001; Weckman et al., 2001; Lu et al., 2015; Muecklich et al., 2023), which also extends to the emerging field of system-level verification in either deterministic or probabilistic sense (Tomlin et al., 2001; Reinhardt, 2013; Hook et al., 2016). Aircraft performance is one of the prime examples for verification of reliability, as they can be modeled in the simulation environment (Heidlauf et al., 2018). However, existing works usually adopt simple approximations which assume the aircraft can be modeled with a point mass (Hu et al., 2020; Guo et al., 2021; Hu et al., 2022) or reduced number of freedom (i.e., Dubins Model) (Dubins, 1957; Molnar et al., 2024). On the other hand, communication latency and complete signal loss are critical events that impact RPAS system reliability, and drastically deteriorate flight performance, especially during autonomous operations. Additionally, the desired level of automation during certain RPAS missions is also an open-ended question to the community. For instance, three levels of control architectures are in service, (i) human-in-the-loop (HITL), where the control system requires continuous and direct human input; (ii) human-on-the-loop (HOTL), where human act as the supervisor to the machine; (iii) fully autonomous, where the RPAS determines procedures to fulfill mission requirements. RPAS are moving objects, proper autonomous functions needs to be put onboard to maintain stability as well as perform basic maneuvers. Studying the impact of C2 link issues helps answer the question of, *how much autonomy and what type of control architecture do we need to be have onboard for RPAS in order to complete the given task?*

One closely-related work was actually done on a within-visual-range (WVR) air-to-air (A2A) dogfight RPAS virtual reality simulator (Thirtyacre, 2021, 2022). The author employed repeated experiments with experienced pilots to test the combat success score, with a set of sparse latency values ranging from 0 up to 1.25 seconds, during high- and low-speed engagement scenarios. The author discovered that when latency cannot be eliminated, conducting

high-speed beyond-line-of-sight (BLOS) engagements may lessen its negative impact, which provides insights for WVR combat in real world. This study makes notably contribution by considering the communication latency in the dynamic dogfight task. However, this study has not considered the impact of complete C2 link loss, while only six latency values are considered in the simulator. Another closely related work studies the impact of communication latency and signal loss on separation assurance of RPAS for autonomous cargo operations (Bulusu et al., 2022). They remarkably consider communication availability by introduce message drop probability (MDP) to approximate the C2 link drop behavior. A sparse set of five values of latency values, and six values of MDP are selected in their simulation. However, only smaller MDP values are selected, and the complete C2 link loss situation is not considered in their study.

To the best of the authors’ knowledge, no existing work has examined the effects of complete communication loss and communication latency simultaneously on the performance of an RPAS within a full six-degree-of-freedom (6DOF) simulation, let alone considered these challenges for high-performance systems (i.e., the F-16 plant). Furthermore, there are no comparable studies that determine the mission success and mission completion time envelopes through extensive Monte Carlo simulations while varying extremely dense latency and availability parameters. Therefore, we highlight the contributions of our work here,

- We examine the concept of RCP and provide the complete mathematical formulation of key metrics on availability and continuity, based on state transition probabilities. The communication availability is modeled as a continuous-time Markov chain (CTMC), which is defined as a continuous-time Markov chain with the *on* and *off* states, with exponential waiting times for each state.
- We propose a new RCP metric, *communicability*, to represent the possibility that a system can support the transmission of messages with a certain duration at any random given time, with a communication latency value.
- We incorporate the communication latency and C2 link loss into the flight simulation of a remotely piloted F-16. The communication latency impacts the time steps to apply the remote control inputs.

- Given the waypoint following task, we generate the mission success rate envelope and mission completion time envelope for successful simulations by conducting extensive Monte Carlo simulations with multiprocessing on a high-performance computer. Mission success is defined as the aircraft reaching the slant range of each waypoint in order. We discover the performance decay behavior by providing a complete study of flight performance under availability and latency variabilities.
- We further generate the figure showing the mission success rate versus communicability under different latency intervals, to help understanding the maximum toleratable latency values for the given waypoint following task.
- We notice an intriguing phenomenon where the remotely piloted F-16 enters an infinite looping behavior while tracking a waypoint during certain latency values with full availability, and slightly decrease or increase the latency can alleviate the issue.

In the remainder of this paper, we provide a literature review of related works in Section 2. Then we look into the concept of RCP, and provide the mathematical formulations of key RCP metrics in Section 3. We briefly introduce the F-16 flight dynamics and control used in the simulation in section 4. Section 5 provides the necessary details on our experiments, with extra discussions in Section 5.4. Section 6 concludes the paper and explain possible future research directions.

2. Literature Review

2.1. Reliability of Communication

The special committee on Future Air Navigation System (FANS) of ICAO has identified the enhancement of communications, navigation, surveillance and air traffic management (CNS/ATM) as one of the first objectives (ICAO AMCP WG-C1/WP8, 2011). C2 link relies on signal propagation to transmit either higher-level operational instructions or immediate flight control parameters for Air-to-Ground or Air-to-Air communications. Signal strength estimation is one of the most critical part of signal propagation (Alsamhi et al., 2018) to ensure the receiver gaining sufficient level of power. Signal propagation can be affected by three main phenomena: reflection, diffraction,



Figure 1: Flight simulation case study in this research. The task has two waypoints: WP1 and WP2. The communication link between the remote piloted station (RPS) and the remotely piloted aircraft (RPA) encounters inbound/outbound latency ε and complete signal loss duration (i.e., availability P_A) during flight, leading to degraded performance on mission completion.

and scattering. Reflection occurs when a signal bounces off large, smooth surfaces, causing multipath fading due to multiple signal paths arriving at different times. Diffraction involves the bending of signals around sharp edges, allowing them to reach shadowed areas not in direct line of sight but causing attenuation in the process. Scattering happens when signals encounter small or irregular objects, dispersing energy in multiple directions and reducing signal strength, yet sometimes assisting in overcoming obstacles by reaching otherwise blocked areas.

Specifically, the term *communication* stands for accurate information transfer between the transmitter and receiver. In this work, voice and data communications are considered within the scope of ATM. Voice communication for Air-to-Ground (A2G) systems within the continental U.S. airspace are two-way between the pilots and the ground stations, achieved by Remote Communication Facilities (RCFs) maintained by FAA. RCFs use Very High Frequency (VHF) and Ultra High Frequency (UHF) antenna transmitters and receivers mounted on buildings or towers. VHF operates from 118 MHz to 136.975 MHz are for civil aviation use, while UHF channel takes

effect from 225 MHz to 400 MHz of military usage (Markus and Eftekari, 2020). High Frequency (HF) aeronautical voice communication also serves A/G communications for a much long range. It is available over international airspace (or continental U.S. only in the case of emergency), which covers frequency from 3 MHz to 30 MHz. Iridium and Inmarsat provide complete or approximate world-wide satellite voice communication (SATVOICE) service in Lower Earth Orbit (LEO) or Geostationary Earth Orbit (GEO). On the other side, data communication refers to textual data providing routes information to the pilots, which also referred as data link. Similar to voice communication, there is HFDL/VDL refers to data link using HF/VHF, as well as Iridium and Inmarsat providing satellite-based data communication (SATCOM) services primarily used in oceanic and remote airspace (The Performance Based Operations Aviation Rulemaking Committee (PARC), 2018).

The concept, *Reliability*, stands for the probability that the system functioning correctly under certain operation conditions over a specific period of time (Villemeur, 1992; Ahmad et al., 2017). The reliability of aviation communication system has been investigated by either the RCP concept by ICAO for manned commercial aviation, or the Required Link Performance (RLP) by the Joint Authorities for Rulemaking of Unmanned Systems (JARUS). RCP and RLP identical key metrics to quantify the reliability of communication systems, transaction time, availability, continuity, and integrity. Similar metrics has also been used in measuring reliability of satellite-based Differential Global Positioning System (DGPS) for maritime navigation (Moore et al., 2002) and other navigation application domains. The detailed explanations and mathematical derivations is given in Section 3, along with our newly proposed metric, *communicability*, to consider the first three key metrics together. For consistency of terminologies, we use RCP to represent RLP throughout this paper.

2.2. Communication Latency

Although RPAS has been deployed in the United States (US) for decades (Gertler, 2012), the latency in C2 link remains an inherent limitation of RPAS operations (Trsek and Maj, 2007). The emerging automation capabilities of RPAS urgently require a thorough understanding of communication latency to flight performance. As shown in Figure 1, the mission we are considering in this work are typically BLOS operations, where the C2 links travel thousands of miles through terrestrial networks and satellites, from the RPS to

RPA (i.e., inbound latency). In return, the RPAS sensor measurements will transmit back to the RPS through the same path (i.e., outbound latency). The latency impacts the measurements of the RPAS true states and what displayed to the RPS, as well as the RP’s control input and RPA receiving the command. As pointed out in the Observation-Orientation-Decision-Action (OODA) loop theory, the capability to operate a faster decision-making process than the opponent will lead to better chance of winning (Brehmer, 2005). Latency is viewed as delays in each step of the OODA loop. Understanding latency impact, especially in highly dynamic environment (i.e., RPAS), is critical and will greatly increase the chance of mission success.

Remotely operated systems, which enable remote operations in environments ranging from remote surgeries to the surfaces of distant planets (i.e., Moon/Mars exploration), are critically affected by latencies in communication links, which reduce the operators’ ability to efficiently control and monitor the robot’s actions (Avgousti et al., 2018; Garcia-Perez and Merino, 2016; Burns et al., 2019; Taylor et al., 2016; Vozar and Tilbury, 2014). Latency originates from various sources, including network delays, processing inefficiencies, and sensory input limitations, and can necessitate suboptimal control strategies (i.e., move-and-wait open-loop), thereby hindering mission success (Lupisella et al., 2018; Vozar et al., 2018). Latency exceeding certain thresholds diminishes situational awareness and adaptability, particularly when it is variable rather than constant, or when it delays feedback to the user rather than the robot (Garcia-Perez and Merino, 2016; Luck et al., 2006). This challenge is significantly magnified over interplanetary distances, where communication delays of up to 20 minutes between Earth and Mars demand advance programming and careful planning of rover operations to mitigate risks and ensure mission objectives are met (Burns et al., 2019; Taylor et al., 2016). As space exploration and other remote applications advance, efforts to reduce or compensate for latency—through low-latency rovers, improved bandwidth, and enhanced levels of autonomy—are seen as essential for enabling human-like precision and creativity, while retaining robotic endurance and safety in hostile or inaccessible environments (Botta et al., 2017; Lupisella et al., 2018). The *move-and-wait* approach is usually employed while communication latency prevents continuous, responsive control, but significantly slow task completion (Sheridan and Ferrell, 1963). Moreover, *move-and-wait* is not possible for RPAS scenarios. Sollenberger et al. (2003) investigates the impact of ground communication system delays to the controller workload, while replacing the aging radio device with

newer models. The HITL simulation study concludes that maximum tolerable ground system delay is 350 ms without impacting the performance on the air traffic controllers.

Possible solutions to fight latencies are improving robot design, employing predictive modeling, and advancing communication technologies. For instance, the typical approach involves inserting a predicted compensatory delay into the feedback loop of the control system, allowing the operator to experience instantaneous synthetic feedback, which is particularly effective when latency is stable and predictable (Zhao et al., 2015; Wang et al., 2017). Emerging high-frequency communication technologies (i.e., 5G), promise both high data throughput and ultra-low latency, enabling more responsive and precise teleoperations (Voigtländer et al., 2017). Additionally, control augmentation strategies such as trajectory prediction (Pang et al., 2021, 2022) can alleviate latency impacts. However, unpredictable external disturbances can make these predictive models unreliable (Chen et al., 2007). Long-term solutions point toward autonomous operations, where vehicles sense, decide, and maneuver without human interference (Byrnes, 2014; Mayer, 2015). A hybrid approach that combines the aforementioned solution strategies may offer promising avenues for mitigating latency, with further necessary improvements.

2.3. Communication Loss

Many factors can cause complete communication signal loss for RPAS, which requires accurate measurement of sensor input (i.e., radar altimeters) for awareness of situations within the area of interest. The sensor data can be inaccurate, delayed, corrupted, or spoofed. Cyber-physical attacks toward communication infrastructures and links is the major source of complete communication signal loss (Dave et al., 2022; Ukwandu et al., 2022). Based on the awareness of the attacker blocking communication channels, we classify them into intentional and unintentional attacks. Intentional attacks toward aviation communication systems include jamming, spoofing, and tampering. Signal jamming refers to deliberately disrupting radio signals using devices that broadcast noise or create interference on the same frequency as aviation communication channels. Spoofing injects false signals to mimic legitimate communication channels to disrupt ATC and pilots. Tempering, also known as man-in-the-middle attack, refers to unauthorized access to the system or even damage physical communication infrastructures. Distributed-Denial-of-Service (DDoS) is viewed as a special form of spoofing by massively in-

jecting false signals into the communication system. Unintentional attacks include the electromagnetic interference (EMI) caused by onboard equipment or passenger electronics, cross-modulation caused the mixing of signals from different frequencies. Space weather events is one example of unintentional attacks towards the aviation communication systems. Space weather events disrupt ionosphere reflections and create blockage of shortwave radio transmissions (Xue et al., 2024). The formation of space weather events is highly unpredictable, as it is related to the moving of particles inside of the Earth’s magnetic field towards the poles caused by solar activities (Tsurutani et al., 2005, 2009, 2022). North Polar Flights traversing the area north of 82°N primarily rely on HF to maintain connection with ground stations, or SATCOM for most remote areas. However, both HF and SATCOM are heavily impacted by space weather events in the area north of 82°N, and even inaccessible for HF bands below 30MHz (Xue et al., 2024). In these scenarios, flights are required to divert or land near the North Pole due to the lack of timely and accurate space weather event prediction.

Few research works considered the issue of communication system loss. A closely related work examines how C2 link latency and communication reliability affect the separation assurance capability of RPAS operating within the national airspace system (Bulusu et al., 2022). Using a generic arrival pattern scenario with three merging flows, the study models latency as the time delay from when air traffic control identifies a required maneuver to when the RPA initiates it, and models reliability as the probability that a control message will fail to be received. The paper discovers that when response times exceed 30 seconds or when message drop probability surpasses 0.2, the chance of loss of safe separation increased. The severity of these impacts varies by RPA aircraft type, highlighting the influence of performance characteristics on safety outcomes. The paper provides detailed insights into how these methods could be applied in future studies as automation in airspace operations continues to grow. Another closely-related work explores the impact of C2 latency on RPA performance during WVR A2A simulated combat in virtual reality environments (Thirtyacre, 2021, 2022). The research focuses on how latency affects decision-making efficiency using Boyd’s OODA Loop, comparing performance under high-speed and low-speed engagements. The author used a repeated-measures design where fighter pilots simulated one-on-one combat with discrete latency levels, and revealed that latency above 0.25 seconds begins to impact performance, with delays over 1.25 seconds leading to severe degradation in control and combat scores. Pilots in high-speed engagements

benefited from consistent turn geometry and sustained higher acceleration loads, which partially offset the latency effects. This study remarkably considers latency effect in a dynamic environment, but fail to include the C2 loss situations.

The existing literature examining the effects of latency and command-and-control (C2) link disruptions on fast-moving vehicles requiring precise, robust control remains limited. While some studies consider latency, they often neglect the impact of C2 link loss altogether or rely solely on probabilistic models, rather than rigorously testing the flight control system with systematically varied inputs. Moreover, current research tends to focus on a narrow set of manually chosen latency values, rather than conducting comprehensive assessments across a dense range of latencies. Although previous work has observed general performance degradation as latency increases, the specific patterns and magnitude of this degradation have not been thoroughly investigated. All of the above discussions motivates this investigation on communication system reliability of RPAS.

3. Required Navigation Performance (RCP)

In this section, we will first introduce the conceptual background of RCP within the Performance-Based Airspace (PBA) and the four major parameters defined by ICAO Section 3.1. Then, we provide the mathematical formulation of RCP parameters in Section 3.2. Lastly, we propose the new metric to represent communication system status, communicability, representing transaction time, availability, and continuity all in one.

3.1. RCP Concept

Performance Based Communication (ICAO, 2006) provides the foundations and specifications to achieve and maintain the **Required Communication Performance (RCP)**. RCP concept is used to specify the required communication performance requirements to support specific functions, operations, and procedures within the performance-based airspace (PBA). While the RCP was proposed by ICAO, JARUS proposed the *Required C2 Link Performance* (RLP) concept for RPAS, to address the emerging need on RPAS communication standardization and provide better terminology to RPAS C2 supporting systems. RLP adopts the same parameters as RCP, except that the performance of C2 link is evaluated on the entire system level (JARUS).

For simplicity, we use RCP throughout the remaining part of the paper. RCP is based on a set of parameters as defined below,

- Transaction Time (TT): The maximum nominal time span required in which the operational communication transaction is completed before alternating to another procedure.
- Availability: The probability of the communication service can be initiated when needed.
- Continuity: Given the service is available, the probability that the communication can be completed within the transaction time.
- Integrity: The probability of transactions completed within the transaction time without detected error.

In RCP, a transaction is the process of the human uses to give clearance, order commands, and send flight information, and is completed based on subjective confidence. Moreover, the transaction time include communication steps such as the speaking time (e.g., averaged 2.6 seconds for pilot and 3.8 seconds for controllers (Sollenberger et al., 2003)) and the reaction time of the controller and the pilot (i.e., 1 second), as well as the Air-to-Ground and Ground-to-Ground signal transmission time. Notably, the European Organisation for Civil Aviation Equipment (EUROCAE) ED136 provides the acceptable maximum latency of $100ms$ from the air traffic controller to the ground stations, $2ms$ for A/G communication, and $50ms$ for radio activation (ICAO ACP-WGF24 WP15, 2011). In the case of multiple transactions, the TT is the time to complete the most stringent transaction. RCP type is the specific label defines the communication transaction performance standard, denoting values for transaction time, availability, continuity and integrity. Five RCP types are prescribed (RCP10, RCP60, RCP120, RCP240, RCP400) (ICAO, 2006). RCP10 standard requires the communication transaction is likely to be finished within 10 seconds, where 10 seconds is the transaction time. It is mostly used for enhancing the aeronautical horizontal separation violation (i.e., 5nm) intervention capability of controller. Continuity can be critical for RCP10, where the transaction is likely to be finished within 10 seconds without the time to repeat the voice messages. To meet RCP10, the transaction should be completed with a single attempt. RCP60 usually complements RCP10 with data communication (i.e., data link). RCP120 and

RCP240 are used for supporting separation violation intervention capability in the extended range of 15nm radius or 30/30 (30nm lateral and 30nm longitudinal). RCP240 is the mandatory for oceanic airspace of application with certain separation standards as noted by the FAA (The Performance Based Operations Aviation Rulemaking Committee (PARC), 2018). Beyond 30/30 separation, RCP400 is the standard for SATVOICE and SATCOM where communication services are provided through HF signal. A recent collaborative study between the FAA and JetBlue Airways conducted in Fall 2017 validated the onboard SATVOICE system is able to satisfy the RCP400 criteria and SATVOICE is viable for RCP400 (The Performance Based Operations Aviation Rulemaking Committee (PARC), 2018). The communication equipment carried by the aircraft should at least satisfy the appropriate required RCP type to receive approval of operations. Other RCP types may also be established based on experience and usage. The development of RCP concept enables regulatory authorities to grant operational approvals for specific areas based on the capability to meet a specified RCP, rather than solely on the installation or carriage of specific communications equipment. The airspace authority prescribes the RCP for a given area of airspace or a specific procedure after determining RCP types, as well as maintaining compliance of RCP among different airspace users.

3.2. Mathematical Formulations

We provide the mathematical formulation of Availability and Continuity in this section. Integrity refers to the trust that can be placed in a data transmission being complete and unaltered, without any undetected loss or corruption of data packets. In this study, we are not concerned with the technical aspects of data packet integrity and only focus on the three other metrics.

We start by defining τ_{msg} as the duration of the message to be transmitted in the communication system (i.e., Transaction Time). We further assume that the signal transition between *on* and *off* states follows the Continuous-Time Markov Chain (CTMC), with exponential waiting times for each state. That is,

- $X(t) = 1$: the *on* state where the service is available.
- $X(t) = 0$: the *off* state where the service is unavailable.

We model the duration of communication availability, T_{on} and the duration of communication unavailability, T_{off} as two independent Exponential random variables,

$$T_{on} \sim \text{Exp}(\lambda_{off}) \quad (1)$$

$$T_{off} \sim \text{Exp}(\lambda_{on}) \quad (2)$$

where the parameters used are defined as,

- λ_{on} : This rate governs the transition from the *off* state ($X(t) = 0$) to the *on* state ($X(t) = 1$). It is the rate at which the communication service becomes available while staying unavailable.
- λ_{off} : This rate governs the transition from the *on* state ($X(t) = 1$) to the *off* state ($X(t) = 0$). It is the rate at which the communication service becomes unavailable while staying available.
- T_{on} : This means that the time duration for which the service stays in the *on* state before switching to *off* is exponentially distributed with rate λ_{off} .
- T_{off} : This means that the time duration for which the service stays in the *off* state before switching to *on* is exponentially distributed with rate λ_{on} .

3.2.1. Availability

Availability is defined as the proportion of time the system is *on* over the long term. Given the definition of the probability of the system states,

- $P_A(t)$: The system is at $X(t) = 1$ state at time t .
- $P_{\bar{A}}(t)$: The system is at $X(t) = 0$ state at time t .

It's clear that $P_A(t) + P_{\bar{A}}(t) = 1$ since there are only two discrete state in such system. Further given the Exponential distributions of T_{on} and T_{off} , we can model the transitions between system states with a continuous-time Markov chain (CTMC) with inflow rate and outflow rate as λ_{on} and λ_{off} , and the corresponding stochastic matrix Q for state transitions can be expressed as,

$$Q = \begin{bmatrix} -\lambda_{on} & \lambda_{on} \\ \lambda_{off} & -\lambda_{off} \end{bmatrix} \quad (3)$$

The rate of change of $P_A(t)$ is defined as the difference between the inflow rate and outflow rate,

$$\frac{dP_A(t)}{dt} = \text{inflow rate} - \text{outflow rate} \quad (4)$$

$$= \lambda_{on} \cdot P_{\bar{A}}(t) - \lambda_{off} \cdot P_A(t) \quad (5)$$

$$= \lambda_{on} \cdot (1 - P_A(t)) - \lambda_{off} \cdot P_A(t) \quad (6)$$

$$= \lambda_{on} - (\lambda_{on} + \lambda_{off}) \cdot P_A(t) \quad (7)$$

The solution of the first-order differential equation has the general form as,

$$P_A(t) = \mathcal{C} \cdot e^{-(\lambda_{on} + \lambda_{off}) \cdot t} + \frac{\lambda_{on}}{\lambda_{on} + \lambda_{off}} \quad (8)$$

with initial condition $P_A(0) = 1$ (assuming the system starts at the *on* state). Then the constant \mathcal{C} is,

$$\mathcal{C} = 1 - \frac{\lambda_{on}}{\lambda_{on} + \lambda_{off}} \quad (9)$$

Finally, the availability is represented as,

$$P_A(t) = \left(1 - \frac{\lambda_{on}}{\lambda_{on} + \lambda_{off}}\right) \cdot e^{-(\lambda_{on} + \lambda_{off}) \cdot t} + \frac{\lambda_{on}}{\lambda_{on} + \lambda_{off}} \quad (10)$$

Notably, the steady state availability is given by the ratio of the expected *on* duration to the total expected cycle time (which is the sum of the expected *on* and *off* times). It is simply the proportion of time that the system is *on* over the infinite horizon ($t \rightarrow \infty$).

$$P_A(t \rightarrow \infty) = \lim_{t \rightarrow \infty} \left(1 - \frac{\lambda_{on}}{\lambda_{on} + \lambda_{off}}\right) \cdot e^{-(\lambda_{on} + \lambda_{off}) \cdot t} + \frac{\lambda_{on}}{\lambda_{on} + \lambda_{off}} \quad (11)$$

$$= \frac{\lambda_{on}}{\lambda_{on} + \lambda_{off}} \quad (12)$$

$$= \frac{\mathbb{E}[T_{on}]}{\mathbb{E}[T_{on}] + \mathbb{E}[T_{off}]} \quad (13)$$

$$(14)$$

3.2.2. Continuity

Continuity is defined as the probability that once the service is available at time t (i.e., *on*), it remains available for the required duration τ_{msg} . If we

discretize τ_{msg} into n steps $\tau_0, \tau_1, \dots, \tau_n$, with infinitesimal time interval $\Delta\tau$. Then we have,

$$\tau_{msg} = \sum_{i=0}^{n-1} \Delta\tau \quad (15)$$

The probability that the system is available on any discretized timestamp is $P(\tau_i)$. By discretizing time duration, we have the continuity expressed as the joint probability at all timestamps,

$$P_C(\tau_{msg}) = P(X(\tau_0) = 1, X(\tau_1) = 1, \dots, X(\tau_n) = 1) \quad (16)$$

$$= P(X(\tau_0) = 1) \cdot P(X(\tau_1) = 1|X(\tau_0) = 1) \cdot P(X(\tau_2) = 1|\{X(\tau_0) = 1 \cap X(\tau_1) = 1\}), \quad (17)$$

$$\dots, P(X(\tau_n) = 1|\{X(\tau_0) = 1 \cap X(\tau_1) = 1, \dots, \cap X(\tau_{n-1}) = 1\}) \quad (18)$$

For Markov process, the joint probability can be simplified by assuming the future state only depends on the current state,

$$P_C(\tau_{msg}) = P(X(\tau_0) = 1) \cdot P(X(\tau_1) = 1|X(\tau_0) = 1), \dots, P(X(\tau_n) = 1|X(\tau_{n-1}) = 1)) \quad (19)$$

$$= P(X(\tau_0) = 1) \cdot \prod_{k=1}^n P(X(\tau_k) = 1|X(\tau_{k-1}) = 1)) \quad (20)$$

$$= P_A(\tau_0) \cdot \prod_{k=1}^n P(X(\tau_k) = 1|X(\tau_{k-1}) = 1)) \quad (21)$$

The transition probability $P(X(\tau_n) = 1|X(\tau_{n-1}) = 1)$ of the Markov process is the probability that the service is at the on state at τ_n given the service is at the on state at τ_{n-1} . That is,

$$P(X(\tau_k) = 1|X(\tau_{k-1}) = 1) = e^{-\lambda_{off} \cdot \Delta\tau}, \quad \forall k \in 1, 2, \dots, n \quad (22)$$

Therefore, the probability that the system remains available for the required duration is,

$$P_C(\tau_{msg}) = P_A(\tau_0) \cdot \prod_{k=1}^n P(X(\tau_k) = 1|X(\tau_{k-1}) = 1)) \quad (23)$$

$$= P_A(\tau_0) \cdot (e^{-\lambda_{off} \cdot \Delta\tau})^{n-1} \quad (24)$$

$$= P_A(\tau_0) \cdot e^{-\lambda_{off} \cdot \sum_{i=0}^{n-1} \Delta\tau} \quad (25)$$

$$= P_A(\tau_0) \cdot e^{-\lambda_{off} \cdot \tau_{msg}} \quad (26)$$

Similarly, assuming the system starts at the on state (i.e., $P_A(\tau_0) = 1$), continuity is expressed as,

$$P_C(\tau_{msg}) = e^{-\lambda_{off} \cdot \tau_{msg}} \quad (27)$$

Notably, this is also the probability that the service maintains the *on* state for at least τ_{msg} before transitioning into the *off* state as,

$$P_C(\tau_{msg}) = P(T_{on} \geq \tau_{msg}) \quad (28)$$

$$= \int_{\tau_{msg}}^{\infty} \text{Exp}(\lambda_{off}) \cdot dx \quad (29)$$

$$= e^{-\lambda_{off} \cdot \tau_{msg}} \quad (30)$$

Continuity is related to the time duration τ_{msg} , for which we desire the service to remain continuously available. This makes it a useful metric for assessing the reliability of service over specific time intervals, independent of when those intervals start, utilizing the memoryless feature of exponential distributions.

3.3. Communicability

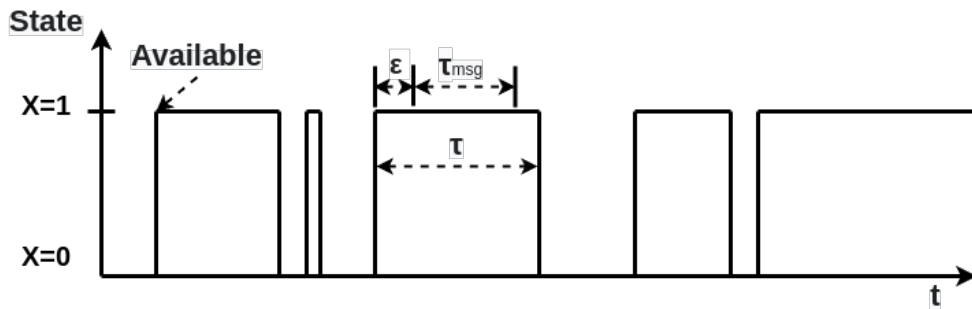


Figure 2: The concept of the control mask square wave.

To further consolidate transaction time, availability, and continuity into a single metric, we propose the *communicability* metric. We define τ as the time since the system most recently became available (as shown in Figure 2), following an exponential decay, and τ_{msg} as the duration of the message to be transmitted in the communication system. ϵ is the latency parameter representing one way system latency in general. The probability density function (PDF) of τ is defined as,

$$f(\tau) = (1 - P_A) \cdot e^{-\frac{\tau}{k}} \quad (31)$$

where the scaling factor k to normalize $f(\tau)$ and k is $\frac{1}{1-P_A}$ by solving,

$$\int_0^{\infty} f(\tau) d\tau = 1 \quad (32)$$

The final representation of $f(\tau)$ becomes,

$$f(\tau) = (1 - P_A) \cdot e^{-(1-P_A)\tau} \quad (33)$$

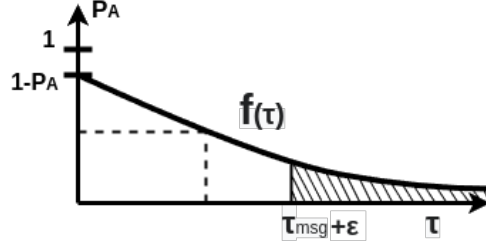


Figure 3: The probability density function of τ

Based on these, we propose a new metric, communicability, representing the probability that a communication system will support the transmission of messages of duration τ_{msg} with latency ε that are initiated at any random time t . The expression for communicability is:

$$P_{\text{comm}} = P_A \cdot \left[\frac{\int_{\tau_{msg} + \varepsilon}^{\infty} (\tau - (\tau_{msg} + \varepsilon)) \cdot f(\tau) d\tau}{\int_0^{\infty} \tau \cdot f(\tau) d\tau} \right] \quad (34)$$

$$= P_A \cdot e^{-(1-P_A) \cdot (\tau_{msg} + \varepsilon)} \quad (35)$$

where P_A is the availability as defined above. In the case where $\lambda_{on} + \lambda_{off} = 1$, the P_{comm} can be expressed as,

$$P_{\text{comm}} = \lambda_{on} \cdot e^{-\lambda_{off} \cdot (\tau_{msg} + \varepsilon)} \quad (36)$$

4. Flight Simulator

In this section, we briefly introduce the 6DOF flight simulation environment used in this research. We adopt the autonomous aerospace verification challenge benchmark, which was released as the basis for analyzing the detailed behavior of autonomous maneuvers for a remotely piloted high performance F-16 Falcon (Heidlauf et al., 2018).

The benchmark model is based on the textbook model, where the performance of F-16 has been extensively studied since the 1970s (Nguyen, 1979; Seto et al., 1999; Stevens et al., 2015). The benchmark uses the linearized version of the nonlinear flight dynamics of the aircraft about a steady-state trim

point (i.e., without gain scheduling), by assuming the autonomous aircraft is operating without sideslip, on a flat earth using the north-east-down frame, and with approximated aerodynamic coefficients. The benchmark model further ignores the leading edge flaps and experimental thrust vectoring control (Sonneveldt, 2006). The aerodynamic coefficients are reasonable approximations for the subsonic flight regime. Euler angle based equations of motion are used, however, they are limited to moderate intensity maneuvers, as they will encounter singularities when the pitch angle θ exceed $\pm\frac{\pi}{2}$, in which case quaternions should be used (Sonneveldt, 2006). Further explanation of the equations of motion is given in Section 4.1.

For the flight controller, the system adopts a *fly-by-wire* control scheme (Favre, 1994), where the aircraft still takes the four standard inputs but the control surfaces are actuated indirectly through the higher-level controller. The higher-level controller (HLC), or Autopilot, adopts integral tracking control, to generate the reference vector as the input to the lower-level controller (LLC) (e.g., Section 5.5 of Stevens et al. (2015)). The LLC decouples the longitudinal and lateral motions and uses two Linear Quadric Regulators (LQRs) with a low-pass filter. Although LQRs have certain limitations on handling high angle-of-attack scenarios and are not as flexible as Nonlinear Dynamic Inversion (NDI) (Yang and Chang, 2024), they were still used in practice by General Dynamics for flight control of the F-16C Fighting Falcon. The specific task we are focusing on is a waypoint following (reaching) task in the NED frame, where the aircraft is expected to reach the current waypoint and then proceed to the next one. The control system adds a performance output to track the given reference inputs and system outputs. This dual-loop controller design uses the digital control implementation of the system-plus-integrator(compensator) augmented state equations to track a command (Stevens et al., 2015). Further explanations are given in Section 4.2.

4.1. Flight Dynamics of the Simulator

In the context of aircraft dynamics and control, navigation equations are the set of equations that determine the aircraft’s position and orientation over time. They relate the aircraft’s motion (velocity and angular rates) to changes in its geographic position (latitude, longitude, altitude) and orientation (roll, pitch, yaw angles). These equations are derived from the kinematic relationships between the aircraft’s body-fixed frame (attached to the aircraft) and the inertial frame (fixed relative to the Earth). They account for the aircraft’s translational and rotational motions to determine how its

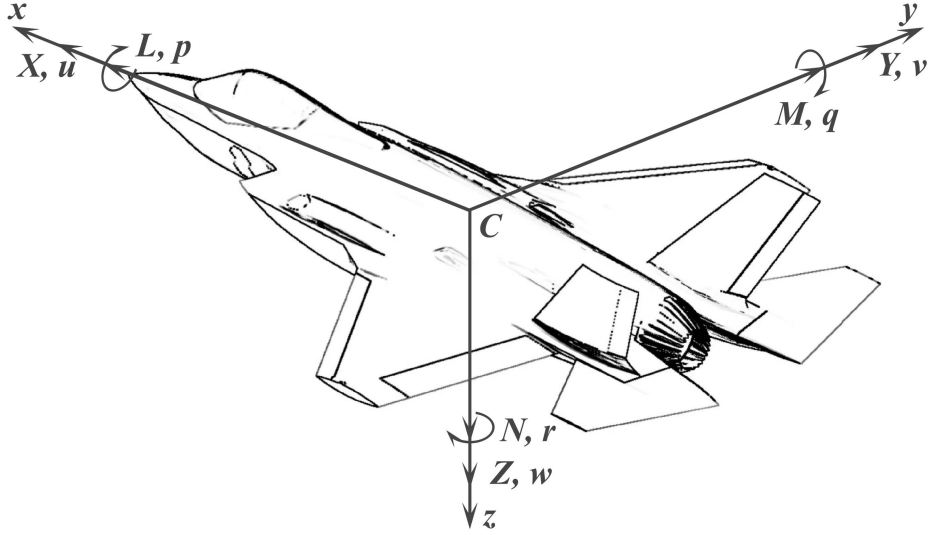


Figure 4: Forces and Moments Acting on the Airplane

position and orientation change over time. The translational motion of the aircraft is governed by Newton's second law,

$$\mathbf{F} = m\mathbf{a} \quad (37)$$

where \mathbf{F} is the vector of forces acting on the aircraft in the body axis frame, including aerodynamic forces \mathbf{F}_d , gravitational forces \mathbf{F}_g and engine thrust forces \mathbf{F}_{th} . In the Earth frame, \mathbf{F}_g is given by:

$$\mathbf{F}_{g,earth} = \begin{bmatrix} 0 \\ 0 \\ mg \end{bmatrix} \quad (38)$$

In the body frame, we need to transform the gravitational force using the aircraft's orientation (Euler angles: roll ϕ , pitch θ , yaw ψ). The gravitational force in body axes becomes:

$$\mathbf{F}_g = mg \begin{bmatrix} -\sin(\theta) \\ \cos(\theta) \sin(\phi) \\ \cos(\theta) \cos(\phi) \end{bmatrix} \quad (39)$$

Without considering thrust vectoring, the force vector can be represented

by,

$$\mathbf{F} = \mathbf{F}_d + \mathbf{F}_g + \mathbf{F}_{th} \quad (40)$$

$$= \begin{bmatrix} X \\ Y \\ Z \end{bmatrix} + mg \begin{bmatrix} -\sin(\theta) \\ \cos(\theta) \sin(\phi) \\ \cos(\theta) \cos(\phi) \end{bmatrix} + \begin{bmatrix} T \\ 0 \\ 0 \end{bmatrix} \quad (41)$$

The acceleration $\mathbf{a} = [\dot{u} \ \dot{v} \ \dot{w}]^T$ can be related to the velocity vector $\mathbf{V} = [u \ v \ w]^T$ (velocity components in the body frame) and the angular rates $\boldsymbol{\omega} = [p \ q \ r]^T$ (roll, pitch, and yaw rates) using the following relation:

$$\dot{\mathbf{V}} = \mathbf{a} + \boldsymbol{\omega} \times \mathbf{V} \quad (42)$$

Thus, the translational dynamics in matrix form are,

$$\begin{bmatrix} \dot{u} \\ \dot{v} \\ \dot{w} \end{bmatrix} = \frac{1}{m} \begin{bmatrix} X + T \\ Y \\ Z \end{bmatrix} + g \begin{bmatrix} -\sin(\theta) \\ \cos(\theta) \sin(\phi) \\ \cos(\theta) \cos(\phi) \end{bmatrix} - \begin{bmatrix} 0 & -r & q \\ r & 0 & -p \\ -q & p & 0 \end{bmatrix} \begin{bmatrix} u \\ v \\ w \end{bmatrix} \quad (43)$$

The Earth frame velocities can be expressed as the product of three rotation matrices that describe the transformation from the body frame to the Earth frame. These rotation matrices are based on the Euler angles: roll (ϕ), pitch (θ), and yaw (ψ).

The relationship between the body frame velocities $[u, v, w]^T$ and the Earth frame velocities $[\dot{x}_e, \dot{y}_e, \dot{h}_e]^T$ can be written as the product of three rotation matrices:

$$\begin{bmatrix} \dot{x}_e \\ \dot{y}_e \\ \dot{z}_e \end{bmatrix} = R_y(\psi)R_p(\theta)R_r(\phi) \begin{bmatrix} u \\ v \\ w \end{bmatrix} \quad (44)$$

$$= \begin{bmatrix} \cos \psi & -\sin \psi & 0 \\ \sin \psi & \cos \psi & 0 \\ 0 & 0 & 1 \end{bmatrix} \begin{bmatrix} \cos \theta & 0 & \sin \theta \\ 0 & 1 & 0 \\ -\sin \theta & 0 & \cos \theta \end{bmatrix} \begin{bmatrix} 1 & 0 & 0 \\ 0 & \cos \phi & -\sin \phi \\ 0 & \sin \phi & \cos \phi \end{bmatrix} \begin{bmatrix} u \\ v \\ w \end{bmatrix} \quad (45)$$

$$= \begin{bmatrix} \cos \theta \cos \psi & \cos \theta \sin \psi & -\sin \theta \\ \sin \phi \sin \theta \cos \psi - \cos \phi \sin \psi & \sin \phi \sin \theta \sin \psi + \cos \phi \cos \psi & \sin \phi \cos \theta \\ \cos \phi \sin \theta \cos \psi + \sin \phi \sin \psi & \cos \phi \sin \theta \sin \psi - \sin \phi \cos \psi & \cos \phi \cos \theta \end{bmatrix} \begin{bmatrix} u \\ v \\ w \end{bmatrix} \quad (46)$$

Rotational dynamics describe how the aircraft rotates about its center of mass in response to external moments. There are two common sets of rotation dynamics equations, (a) kinematic equations relate angular velocities to the rate of change of the Euler angles; (b) moment equations bridge moments to angular accelerations.

For kinematic equations, the body frame angular velocities (p, q, r) are related to the time derivatives of the Euler angles (ϕ, θ, ψ) via the following transformation:

$$\begin{bmatrix} \dot{\phi} \\ \dot{\theta} \\ \dot{\psi} \end{bmatrix} = \begin{bmatrix} 1 & \sin \phi \tan \theta & \cos \phi \tan \theta \\ 0 & \cos \phi & -\sin \phi \\ 0 & \sin \phi / \cos \theta & \cos \phi / \cos \theta \end{bmatrix} \begin{bmatrix} p \\ q \\ r \end{bmatrix} \quad (47)$$

where,

- $\dot{\phi}, \dot{\theta}, \dot{\psi}$ are the time derivatives of the Euler angles (roll, pitch, and yaw rates).
- p, q, r are the body angular velocities about the $x, y,$ and z -axes.

In rotational dynamics, the rotational motion of the aircraft is governed by Euler's rotational equations:

$$\mathbf{M} = \mathbf{I}\dot{\omega} + \omega \times (\mathbf{I}\omega) \quad (48)$$

where $\mathbf{M} = [L \ M \ N]^T$ is the vector of roll, pitch, and yaw moments, $\omega = [p \ q \ r]^T$ is the angular velocity in the body frame, $\dot{\omega} = [\dot{p} \ \dot{q} \ \dot{r}]^T$ is the angular rates, while $\mathbf{I} = \begin{bmatrix} I_{xx} & -I_{xy} & -I_{xz} \\ -I_{xy} & I_{yy} & -I_{yz} \\ -I_{xz} & -I_{yz} & I_{zz} \end{bmatrix}$ is the inertia of the aircraft. From Equation (48), the equation of motion for angular velocity ω is,

$$\dot{\omega} = \mathbf{I}^{-1}(\mathbf{M} - \omega \times \mathbf{I}\omega) \quad (49)$$

This can be simplified as follows,

$$\dot{p} = (C_1 r + C_2 p)q + C_3 L + C_4 N \quad (50)$$

$$\dot{q} = C_5 p r - C_6 (p^2 - r^2) + C_7 M \quad (51)$$

$$\dot{r} = (C_8 p + C_2 r)q + C_4 L + C_9 N \quad (52)$$

where,

$$C_1 = \frac{(I_{yy} - I_{zz})I_{zz} - I_{xz}^2}{\Gamma}, C_2 = \frac{I_{xz}(I_{xx} - I_{yy} + I_{zz})}{\Gamma}, C_3 = \frac{I_{zz}}{\Gamma} \quad (53)$$

$$C_4 = \frac{I_{xz}}{\Gamma}, C_5 = \frac{I_{zz} - I_{xx}}{I_{yy}}, C_6 = \frac{I_{xz}}{I_{yy}} \quad (54)$$

$$C_7 = \frac{1}{I_{yy}}, C_8 = \frac{(I_{xx} - I_{yy})I_{xx} - I_{xz}^2}{\Gamma}, C_9 = \frac{I_{xx}}{\Gamma} \quad (55)$$

$$\Gamma = I_{xx}I_{zz} - I_{xz}^2 \quad (56)$$

Specifically, the aerodynamic force vector \mathbf{F}_d and aerodynamic moment vector \mathbf{M} are computed by,

$$\mathbf{F}_d = \begin{bmatrix} X \\ Y \\ Z \end{bmatrix} = \bar{q}S \begin{bmatrix} C_{XT}(\alpha, \beta, p, q, r, \delta_e, \delta_a, \delta_r) \\ C_{YT}(\alpha, \beta, p, q, r, \delta_e, \delta_a, \delta_r) \\ C_{ZT}(\alpha, \beta, p, q, r, \delta_e, \delta_a, \delta_r) \end{bmatrix} \quad (57)$$

$$\mathbf{M} = \begin{bmatrix} L \\ M \\ N \end{bmatrix} = \bar{q}S \begin{bmatrix} bC_{LT}(\alpha, \beta, p, q, r, \delta_e, \delta_a, \delta_r) \\ \bar{c}C_{MT}(\alpha, \beta, p, q, r, \delta_e, \delta_a, \delta_r) \\ bC_{NT}(\alpha, \beta, p, q, r, \delta_e, \delta_a, \delta_r) \end{bmatrix} \quad (58)$$

where the total aerodynamic force coefficients C_{XT}, C_{YT}, C_{ZT} and total moment coefficients C_{LT}, C_{MT}, C_{NT} are usually obtained from wind-tunnel tests of a scaled aircraft model. In this case, we use the aerodynamic coefficients provided in Appendix A.8 of Stevens et al. (2015) with polynomial interpolations from (Morelli, 1998). The detailed calculation of the coefficients is provided in Sonneveldt (2006). It worth noting that leading edge flaps (e.g., δ_F) are not considered as in Yang and Chang (2024), resulting in a low-fidelity aircraft model used for demonstration and verification purposes as in Stevens et al. (2015).

These 12 equations of motion describe the aircraft's position, velocity, and orientation in typical 6DOF flight simulation models. In this research, we have the 13th additional equation of motion that models the thrust lag for a turbojet engine. The state variable associated with this equation is the actual engine thrust $\delta_t(t)$. The thrust lag function refers to the dynamics of how the aircraft's thrust changes in response to throttle inputs from the pilot. This is due to the physical inertia of the engine and delays in the fuel control system. The thrust produced by an engine doesn't change instantaneously

when the throttle is adjusted, as it takes a time for the engine to spool up (increase thrust) and spool down (decrease thrust). This delay is often modeled as a first-order lag system of the form,

$$\dot{\delta}_t = \frac{1}{\kappa} (\delta_t^{\text{cmd}} - \delta_t) \quad (59)$$

where δ_t^{cmd} is the commanded thrust (i.e., the thrust the pilot intends based on the throttle position). κ is the time constant of the thrust lag, representing how quickly the engine can respond to changes in throttle position. A small τ means a fast response (minimal lag), while a larger τ means a slower response (more lag). $\dot{\delta}_t$ is the time derivative of the thrust, or the rate of change of thrust.

This completes the equations of motion for the aircraft position, velocity, orientation, and engine response. Higher-fidelity F-16 flight simulation models may consider leading edge flaps and coupling between longitudinal and lateral dynamics (Sonneveldt, 2006).

4.2. Controller Design

We are interested in a waypoint following task where the flight controller follows a reference command signal provided by an autopilot. The control system adopts the design called system-plus-integrator(compensator) with augmented states of the following form,

$$\dot{\mathbf{x}}(t) = A \cdot \mathbf{x}(t) + B \cdot \mathbf{u}(t) + G \cdot \mathbf{r}(t) \quad (60)$$

$$\mathbf{y}(t) = C \cdot \mathbf{x}(t) + F \cdot \mathbf{r}(t) \quad (61)$$

$$\mathbf{z}(t) = H \cdot \mathbf{x}(t) \quad (62)$$

and the control outputs of the form,

$$\mathbf{u}(t) = -K \cdot \mathbf{y}(t) \quad (63)$$

with $\mathbf{x}(t) \in \mathbb{R}^n$ the state variables, $\mathbf{u}(t) \in \mathbb{R}^m$ the control inputs, and $\mathbf{y}(t) \in \mathbb{R}^p$ the measured outputs. The optimal feedback control gain matrix $K \in \mathbb{R}^{m \times p}$ is determined by the design procedure. If the objective is to guarantee stability by driving any initial condition errors to zero, then the optimal control input $\mathbf{u}(t)$ to optimize the quadratic cost of,

$$\min \mathcal{J} = \frac{1}{2} \int_0^\infty (\mathbf{x}(t)^T Q \mathbf{x}(t) + \mathbf{u}(t)^T R \mathbf{u}(t)) dt \quad (64)$$

is desired, where Q and R are penalty metrics in symmetric positive-semidefinite forms (i.e., $\mathcal{J} \geq 0$). The optimal solution can be solved with Riccati equation, or gradient-based approach when an analytical solution is infeasible (Choi and Seo, 1999; Ashraf et al., 2018; Priyambodo et al., 2020).

Moreover, this flight simulator adopts a cascading control scheme where an outer loop (Autopilot) responsible for high-level tasks (i.e, waypoint navigation), and an inner loop (LLC) ensures precise tracking of the Autopilot’s reference commands $\mathbf{r}(t)$. The Autopilot computes $\mathbf{r}(t)$ based on the aircraft’s current state and the desired waypoints, providing heading adjustment, altitude changes, and airspeed maintenance. The LLC uses an LQR controller with integral augmentation to compute control inputs that minimize tracking errors and ensure robustness. Lastly, elements of the feedback gain matrix K coupling lateral and longitudinal states are regulated to zero, such that the coupling between certain input-output pairs are eliminated (i.e., decoupled lateral and longitudinal motion controls). This is also known as the constrained output feedback design. The detailed derivation of the compensator dynamics with augmented states can be found from Section 5.4 to Section 5.7 of Stevens et al. (2015).

4.2.1. Higher-Level Control

Higher-level control is referred to as Autopilot in the benchmark. Autopilot provides *pilot relief* such that the pilot does not need to pay continuous attention to controlling the aircraft, especially when the aircraft is designed slightly unstable (Stevens et al., 2015). Autopilot provides automatic control systems to handle certain pilot relief functions (i.e., altitude holding) and special procedure functions (i.e., automatic landing). The Autopilot uses Proportional-Derivative (PD) controllers to compute high-level reference commands for the aircraft’s heading, roll angle, altitude, and airspeed. These reference commands are then passed to the Low-Level Controller (LLC), which handles the precise tracking of these commands using an LQR with integral action. Autopilot has four control objectives, (i) heading control; (ii) roll angle control; (iii) altitude control; (iv) airspeed control.

For our waypoint following task, we have the waypoint autopilot, which uses geometrically derived guidance based on the kinematic relationships (Lee et al., 2010; Jensen, 2011; He et al., 2019) for RPAS navigation. Given the current waypoint $\text{WP} = (x_{wp}, y_{wp}, z_{wp})$, and the current aircraft states

(x_e, y_e, z_e) , all in the NED frame, we have the distance to the waypoint as,

$$\Delta_x = x_{wp} - x_e, \quad \Delta_y = y_{wp} - y_e, \quad \Delta_z = z_{wp} - z_e. \quad (65)$$

The desired heading ψ^{cmd} to the waypoint WP is computed by,

$$\psi^{\text{cmd}} = \frac{\pi}{2} - \tan^{-1} \left(\frac{\Delta_y}{\Delta_x} \right) \quad (66)$$

where the heading $\psi = 0$ is aligned along the x-axis.

Heading control uses variables $\psi, \psi^{\text{cmd}}, r$ where ψ and ψ^{cmd} are the aircraft current and reference yaw angles respectively, and ϕ^{cmd} is the reference roll angle provided by heading control. In heading control, $e_\psi = \psi^{\text{cmd}} - \psi$ computes the heading error between the desired heading to the waypoint and the current heading where the PD controller is applied to the heading error to calculate the desired roll angle ϕ^{cmd} that steers the aircraft towards the waypoint as,

$$\phi^{\text{cmd}} = k_{\psi_p} e_\psi - k_{\psi_d} r = k_{\psi_p} (\psi^{\text{cmd}} - \psi) - k_{\psi_d} r \quad (67)$$

where k_{ψ_p} is the proportional gain for heading error, and k_{ψ_d} is the derivative gain for yaw rate damping. The derivative term uses the yaw rate r to provide damping, preventing overshoot and improving stability. The desired roll angle is limited to ensure the aircraft does not exceed safe bank angles.

Roll angle control considers $\phi, \phi^{\text{cmd}}, p$ by calculating the error between the current and desired roll angle $e_\phi = \phi^{\text{cmd}} - \phi$ with PD control,

$$p_s^{\text{cmd}} = k_{\phi_p} e_\phi - k_{\phi_d} p = k_{\phi_p} (\phi^{\text{cmd}} - \phi) - k_{\phi_d} p \quad (68)$$

where k_{ϕ_p} is the proportional gain for roll angle error, and k_{ϕ_d} is the derivative gain for roll rate damping. This PD control calculates the desired roll rate in the stability axis p_s^{cmd} needed to achieve the desired roll angle, as the reference for controlling aileron deflection.

Altitude control calculates the desired normal load factor N_z^{cmd} needed to achieve the desired altitude, with a PD control on the altitude error e_{z_e} and rate of climb/descent \dot{z}_e with,

$$N_z^{\text{cmd}} = k_{z_p} e_{z_e} - k_{z_d} \dot{z}_e = k_{z_p} (z_{e\text{cmd}} - z_e) - k_{z_d} \dot{z}_e \quad (69)$$

where $e_{z_e} = z_{e\text{cmd}} - z_e$ is the altitude error and $\dot{z}_e = V_t \sin(\gamma)$ is the projection of airspeed V_t onto the flight path angle γ . Similarly, proportional gain is applied to the altitude error, and a derivative gain is added to \dot{z}_e .

Airspeed control is the proportional control (P-Control) for the throttle command,

$$\delta_t^{\text{cmd}} = k_{V_t} e_{V_t} = k_{V_t} (V_t^{\text{cmd}} - V_t) \quad (70)$$

which controls the airspeed error e_{V_t} between the desired airspeed (V_t^{cmd}) and the current airspeed (V_t). δ_t^{cmd} directly adjusts the engine thrust output.

Autopilot outputs the reference vector $\mathbf{r} = [N_z^{\text{cmd}}, p^{\text{cmd}}, N_{yr}^{\text{cmd}}, \delta_t^{\text{cmd}}]$ to the lower level controller. The Autopilot sets $N_{yr}^{\text{cmd}} = 0$ in standard maneuvers by default to avoid introducing sideslip or yawing motion, while the lower level control can adjust the rudder deflection δ_r to maintain coordinated flight.

4.2.2. Lower-Level Control

LLC handles the precise tracking of reference commands by computing the necessary control surface deflections and throttle settings, to ensure that the aircraft's response closely follows the reference commands. LLC operates by a Linear Quadratic Regulator (LQR) with integral actions for integral tracking control. LQR with integral tracking control can be achieved by adding integral state errors, resulting in the augmented states. Furthermore, in digital control implementations, the control of lateral and longitudinal motions is separated into two LQR controllers.

For longitudinal motion, the short-period approximation to the aircraft dynamics is linearized around the nominal flight condition, as referenced in Table 3.6-3 of (Stevens et al., 2015). The states of interests are $\mathbf{x}_{\text{long}} = [\alpha, q, \int e_{N_z} dt]^T$, and $\mathbf{y}_{\text{long}} = [\alpha, q, N_z]^T$, where $\int e_{N_z} dt$ is the integral of the normal acceleration error. $e_{N_z} = N_z^{\text{ref}} - N_z$ is the difference between the reference normal acceleration from the Autopilot and the measured normal acceleration. The control input for longitudinal motion is the elevator deflection in radians $\mathbf{u}_{\text{long}} = [\delta_e]$.

For lateral motion, a separated LQR is introduced with the state variables $\mathbf{x}_{\text{lat}} = [\beta, p, r, \int e_{\psi} dt, \int e_{N_{yr}} dt]^T$, and $\mathbf{y}_{\text{lat}} = [\beta, p, r, \psi, N_{yr}]^T$ with control inputs $\mathbf{u}_{\text{lat}} = [\delta_a, \delta_r]^T$. Similar to the longitudinal controller, the lateral controller uses state feedback combined with error integrals to ensure accurate tracking and disturbance rejection. The control inputs are computed as a linear combination of the current states and the integral of the error states.

The LQR controller ensures optimal performance for the longitudinal dynamics of the F-16 aircraft, focusing on minimizing steady-state errors in normal acceleration while considering control effort. The control law for \mathbf{u}_{long} and \mathbf{u}_{lat} is thus given as Equation (63), with corresponding control gain matrices K_{long} and K_{lat} .

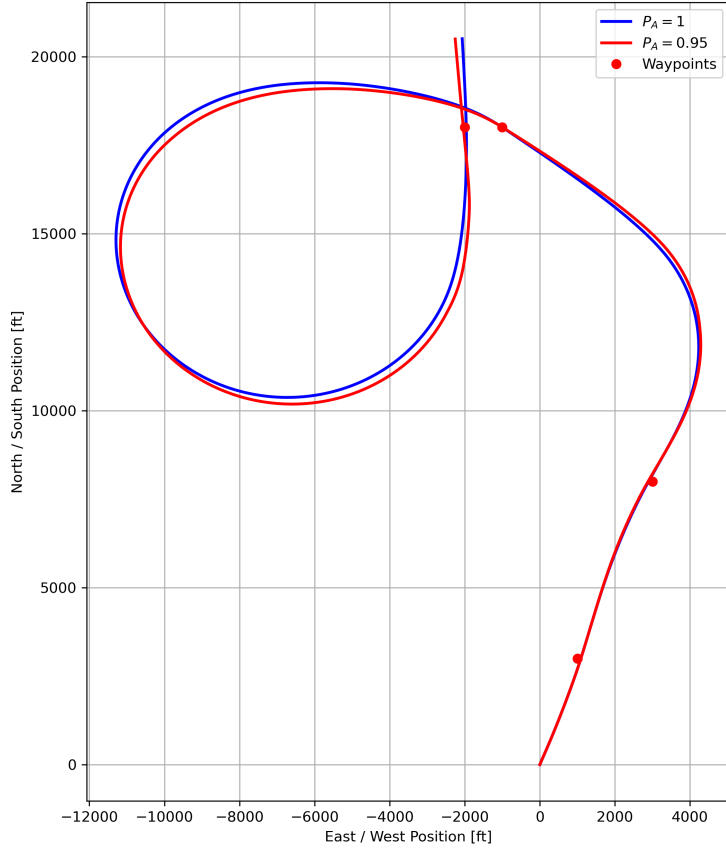


Figure 5: Aircraft trajectory in the vertical plane when comparing $P_A = 1$ and $P_A = 0.95$ with no latency in both cases. For a given $P_A = 0.95$, we first generate the signal state masks square wave for the entire simulation duration Figure 2. Then, apply to the mask to $\mathbf{u}(t)$ to inference the state derivatives.

Following the formulation in Section 3.2, we simulate communication C2 link loss with CTMC between the *on* and *off* states Figure 6. The overhead aircraft trajectory from two simulation runs with $P_A = 1$ and $P_A = 0.95$ is also shown Figure 5, along with a comparison of higher-level control inputs (Figure 8) and lower-level control inputs (Figure 9). The mission is defined as a waypoint following task, where the RPAS is commanded to reach a mini-

mum slant range to each waypoint before proceeding to the next. The RPAS starts from the origin, while the airspace of interest is $[-12, 000, 4, 000]$ feet on the east/west direction, and $[0, 20, 000]$ feet to the north/south direction. The altitude range is around $[3, 800, 4, 600]$ feet with V_t between $[535, 555]$ feet/second (Figure 7). We choose to regulate first three higher-level reference values $\mathbf{r} = [N_z^{\text{cmd}}, p^{\text{cmd}}, N_{yr}^{\text{cmd}}, \delta_t^{\text{cmd}}]$ to 0 once the C2 link is lost. The objective of regulating these reference values to zero is to make sure the F-16 can return to a steady straight and level flight once the RP connection is lost.

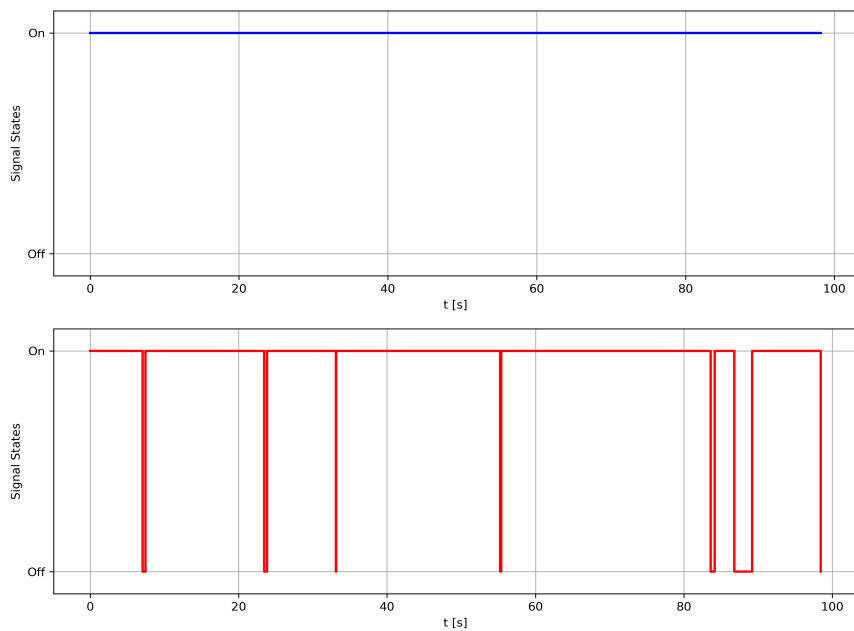
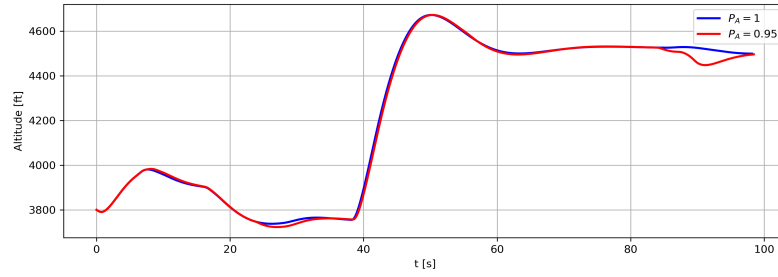
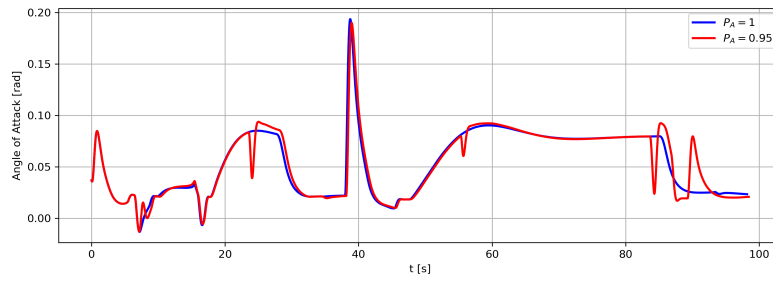


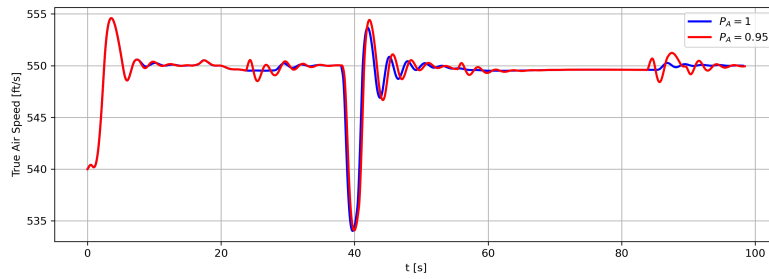
Figure 6: Control signal states during simulation.



(a) Altitude along trajectory.

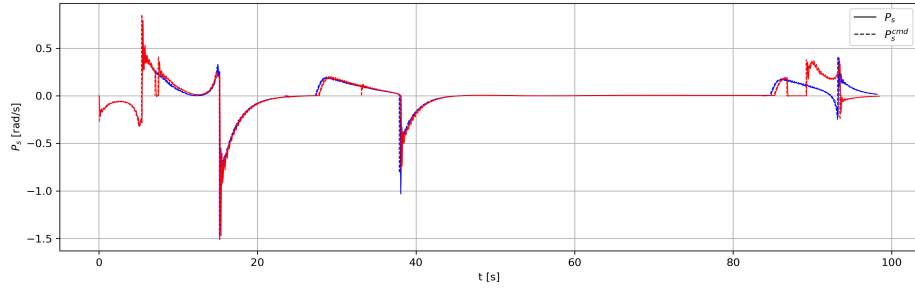


(b) Angle of Attack α versus simulation time.

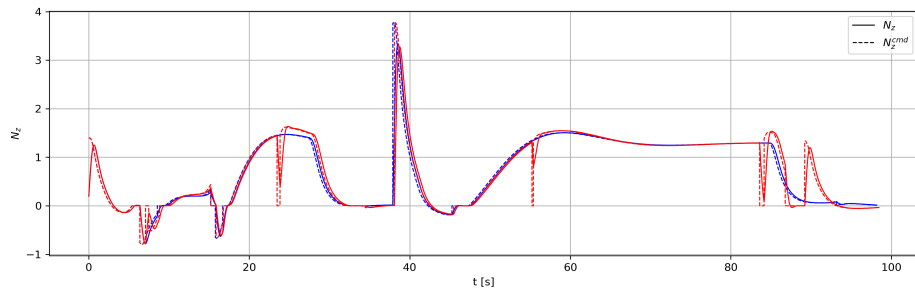


(c) Airspeed V_t along trajectory.

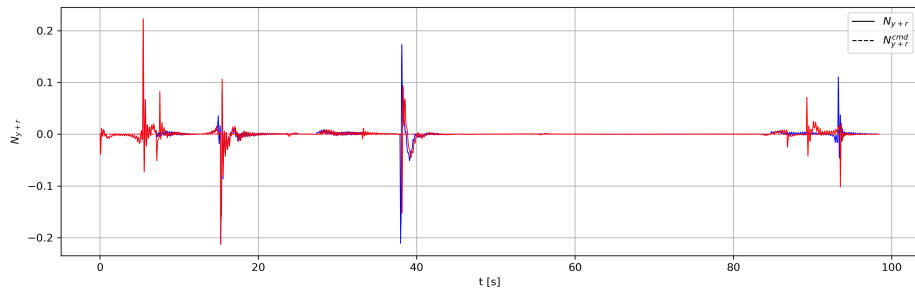
Figure 7: Altitude, angle of attack, and airspeed under different communication availabilities during the waypoint reaching simulation.



(a) Stability roll rate p_s along trajectory .

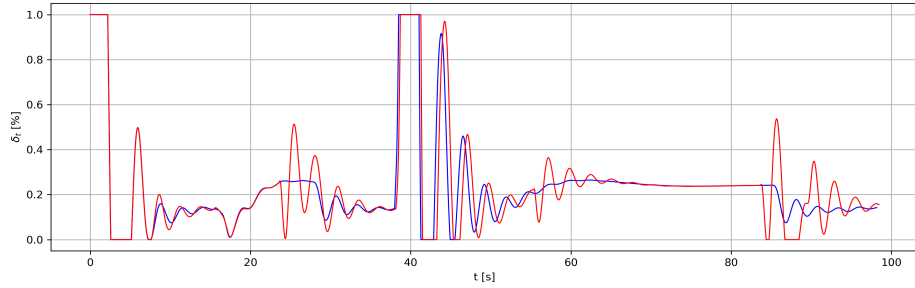


(b) Normalized load factor N_z along trajectory .

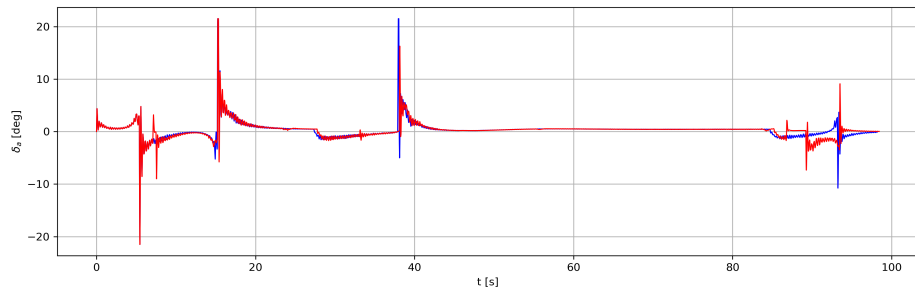


(c) Sum of the side acceleration and yaw rate $N_y + r$ along trajectory.

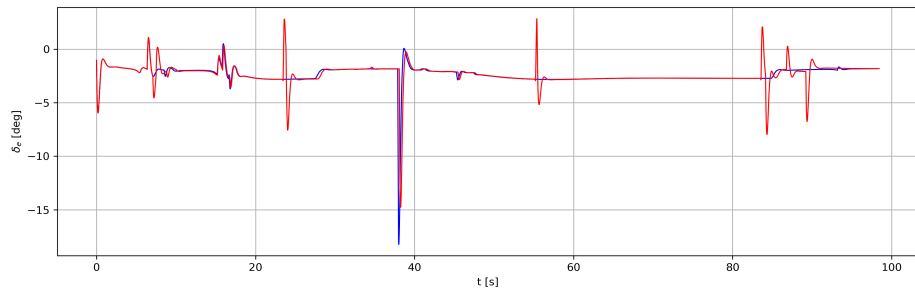
Figure 8: Higher-level control variables under different communication availabilities during the waypoint reaching simulation.



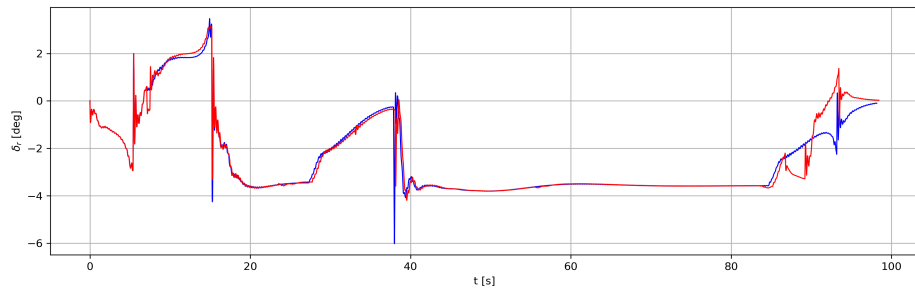
(a) Throttle power command δ_t along trajectory.



(b) The aileron surface deflection δ_a along trajectory.



(c) The elevator surface deflection δ_e along trajectory.



(d) The rudder surface deflection δ_r along trajectory.

Figure 9: Lower-level control variables under different communication availabilities during the waypoint reaching simulation.

5. Monte Carlo Simulations

In this section, we show the details of our Monte Carlo simulation experiments. We start by introducing the definition of the mission in this study. Then, we explain the steps to include communication loss and latency to the RPAS simulation. We further give necessary technical details on the Monte Carlo simulations to generate the communicability performance envelopes – the key concept we intend to introduce with this study. As a reference, Section 5.1 shows the flowchart of the procedures.

5.1. Definition of Mission Success

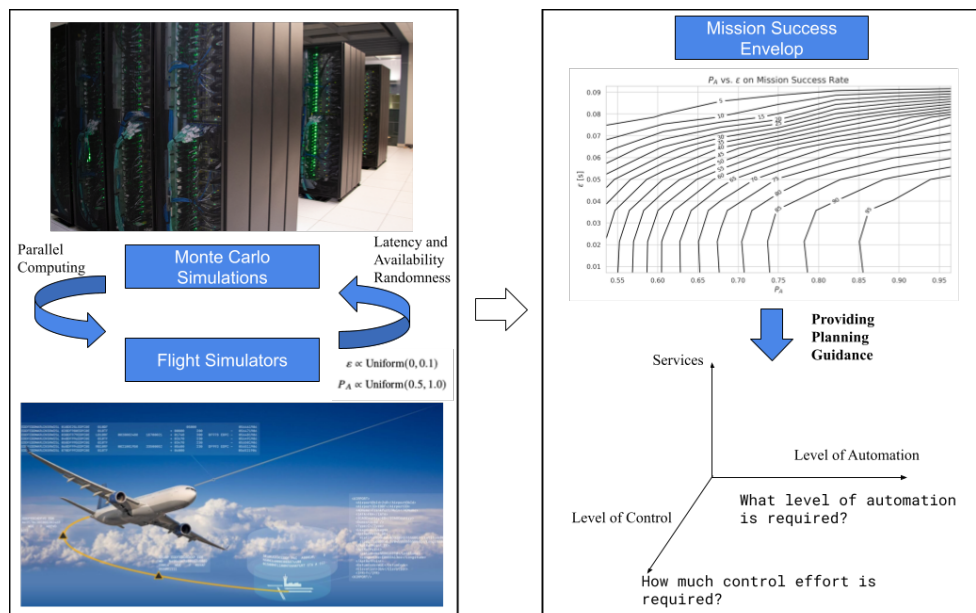


Figure 10: Flowchart of the experiment.

The mission is defined as the waypoint following task in the 3D airspace. Following the notations and derivations used for HLC in Section 4.2.1, we further compute the slant range R by the L^2 distance between the current waypoint and the current position (e.g., $R = \sqrt{\Delta_x^2 + \Delta_y^2 + \Delta_z^2}$). The simulation checks the slant range to each current waypoint, and switches to the next waypoint only if the condition $R < R_{\text{threshold}}$ is met. Once all waypoints are reached, the simulation changes the mode to *Done*, and sets ψ^{cmd} to 0 in HLC to maintain a level flight. Mission completion is defined as the RPAS

reaches all given waypoint in the current scenario with a *Done* status from the simulator. Specifically, we select two waypoint scenarios to represent a hard case and a simple case as in Figure 11. Figure 11a is considered the hard case with 4 waypoints and requires a minimum radius turn of RPAS, while Figure 11b is the simple scenario.

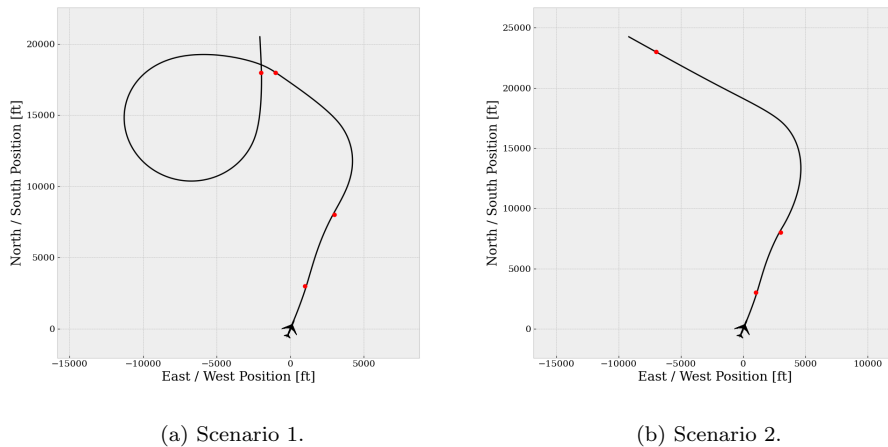


Figure 11: Flight trajectory in the vertical plane for two scenarios used in this work. The first scenario is considered the hard case with 4 waypoints and requires a minimum radius turn of the RPAS. The second scenario is the simple case with three waypoints.

5.2. Mission Success Envelope

	P_A		ε		Number of Simulations
	Distribution	Step	Distribution	Step	
Scenario 1	Uniform(0.5, 1)	1e-3	Uniform(0, 0.1)	1e-3	1,124,413
Scenario 2	Uniform(0.5, 1)	1e-3	Uniform(0, 0.1)	1e-3	1,109,958

Table 1: Monte Carlo Simulation random parameters for two waypoints following scenarios. For each simulation run, we random sample P_A from Uniform(0.5, 1), and ε from Uniform(0, 0.1). A total of over one million sample results are collected for each scenario.

We assume the inbound and outbound latency are identical, thus the total delay is assumed to be 2ε . For the given simulation time step t , the control vector $\mathbf{u}(t)$ is,

$$\mathbf{u}(t) = X(t) \cdot \mathbf{u}(t - 2\varepsilon) \tag{71}$$

where $X(t)$ is the signal state at time t . There are two source of uncertainty in each simulation run, the latency ε , and the signal states $X(t)$ obtained from CTMC with transition probability P_A between the *on* and the *off* states. From Section 3.2, the signal availability is determined by the duration of the *on* state and the *off* states, which follows exponential distributions governed by λ_{on} and λ_{off} . Further assuming $\lambda_{on} + \lambda_{off} = 1$, we have $P_A = \lambda_{on}$. Thus, the random variables for Monte Carlo simulations narrow down to P_A and ε . Table 1 provides the detailed selection of the random variables. We choose the dense grid interval of 0.001 for both P_A and ε .

The simulation was completed on a high-performance workstation with Intel Xeon w9-3495X processor with 56 cores, 112 threads, and a maximum turbo frequency of up to 4.8 GHz. We collect slightly over 1 million Monte Carlo Simulation samples for each scenario, utilizing the multiprocessing tools (Aziz et al., 2021). We further store the Boolean indicating whether the waypoint following mission is completed, and the mission completion time if completed.

5.2.1. Mission Success Rate

Mission success rate is a straightforward performance indicator. It quantifies how frequently an operation meets the intended goals, thereby informing engineers or decision-makers on overall system reliability expectations, and the regions in need of improvement (Chamberlain, 1966; Jacklin, 2019; Zhao et al., 2020). In this work, mission success rate is calculated as the ratio between completed simulations and total number of simulations for any given parameter pair ε and P_A . It stands for the percentage or proportion of attempts that meet the predefined success criteria given above.

As shown in Section 5.2.1, the probability of mission success decreases monotonically as the random variables ε and P_A increase. Moreover, once these variables exceed a certain threshold, the success rate deteriorates sharply, with the rate of deterioration continuing to accelerate thereafter.

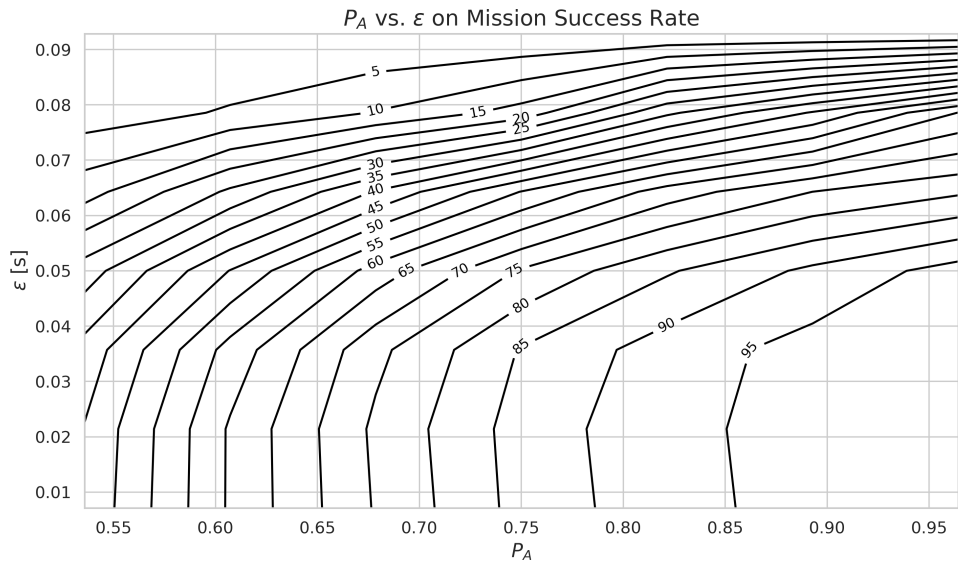


Figure 12: An example of the figure showing the contour lines on mission success levels. Mission success rate percentage is marked on the contour lines.

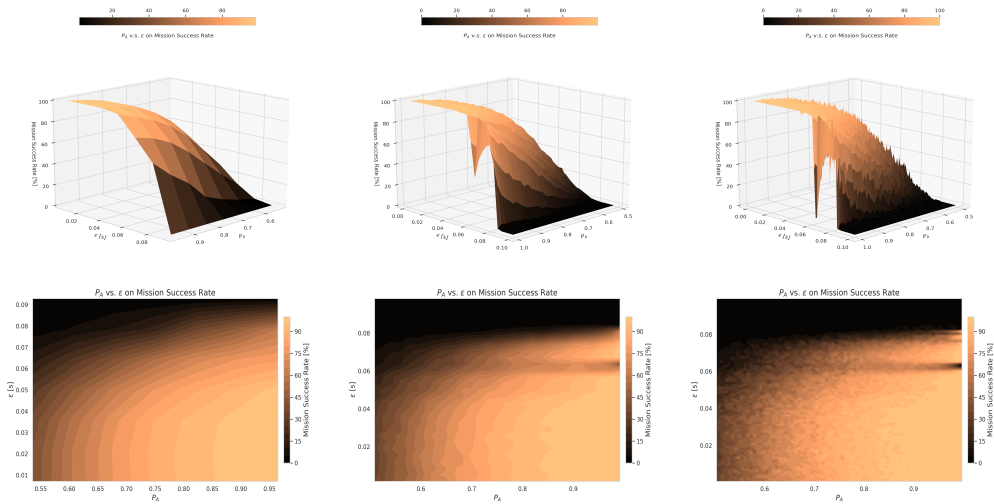


Figure 13: Scenario 1: mission success surface envelop (top row) and mission success surface contour (bottom row).

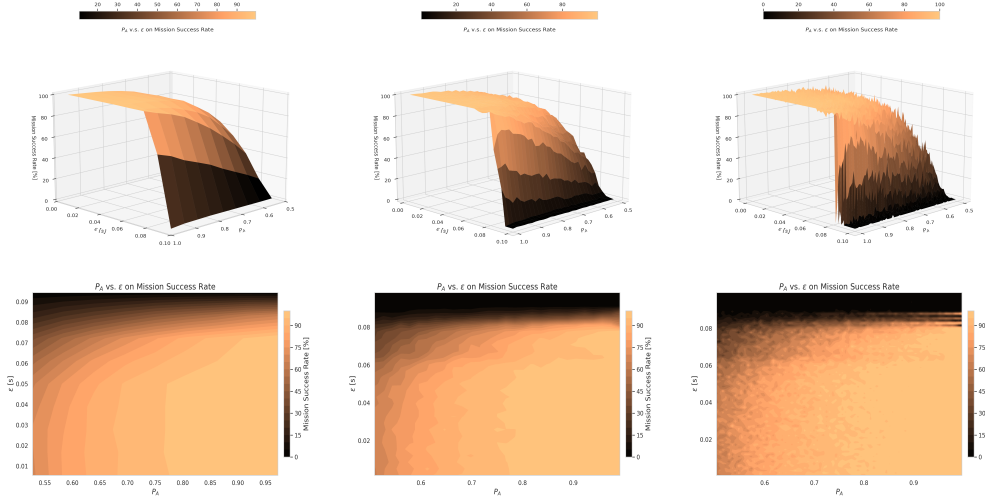


Figure 14: Scenario 2: mission success surface (top row) and mission success surface contour (bottom row).

Figure 13 and Figure 14 present more results on both scenarios. The top row is the mission success envelop in 2D space (i.e., surface), and the bottom row is for the 3D space (i.e., contour). The resolution (e.g., the number of histogram bins on the x-axis and y-axis) increases from left column to right column. Complex scenarios clearly requires lower latency and higher availability to achieve the same level of mission success, but the performance deterioration behavior remains. The phase margin measure of stability and robustness, attainable via Nyquist and Bode analysis, provides an insight into the deterioration of performance with increasing latency. The closed-loop system stability and performance degrades when the control system is pushed to its margins (Brinker and Wise, 1996; Pachter et al., 1996; Hess and Peng, 2018). More theoretical analysis on verifying the Nyquist stability criterion under increased latency is highly desired, and is listed as a topic of future study.

Additionally, the higher resolution mission success envelope of scenario 1 reveals the behavior where certain latency values ϵ can fail the mission, even with very high availability (i.e., $P_A = 1$). This pattern is not significant in the simpler scenario. We name it *latency blockage*. Slightly decreasing or increasing latency alleviates the issue. More analysis on *latency blockage* is given in Section 5.4.

5.2.2. Mission Completion Time

Mission completion time is another metric to quantify the RPAS performance, especially in success simulations. Similar to the mission success rate, we present the mission completion surfaces and contours in Figure 15 and Figure 16. In general, the mission completion time is lower for better communication situations, and the simpler scenario requires less time to complete the mission. In the simpler scenario (i.e., scenario 2), the mission completion time increases monotonically as latency rises and availability falls. However, the behavior in scenario 1 is more complex. While P_A exerts a strictly monotonic influence on the mission completion time, ε is again subject to *latency blockage*.

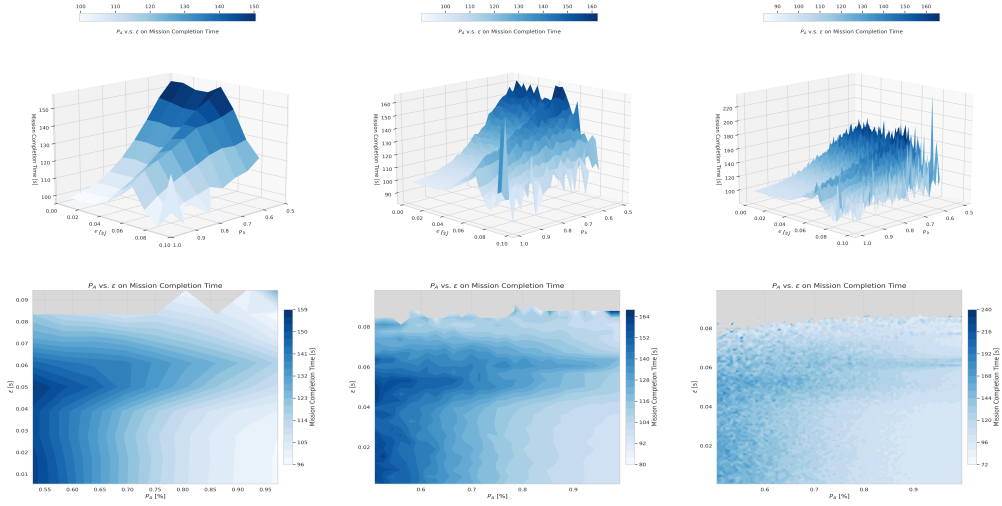


Figure 15: Scenario 1: mission completion time surface (top row) and mission completion time contour (bottom row).

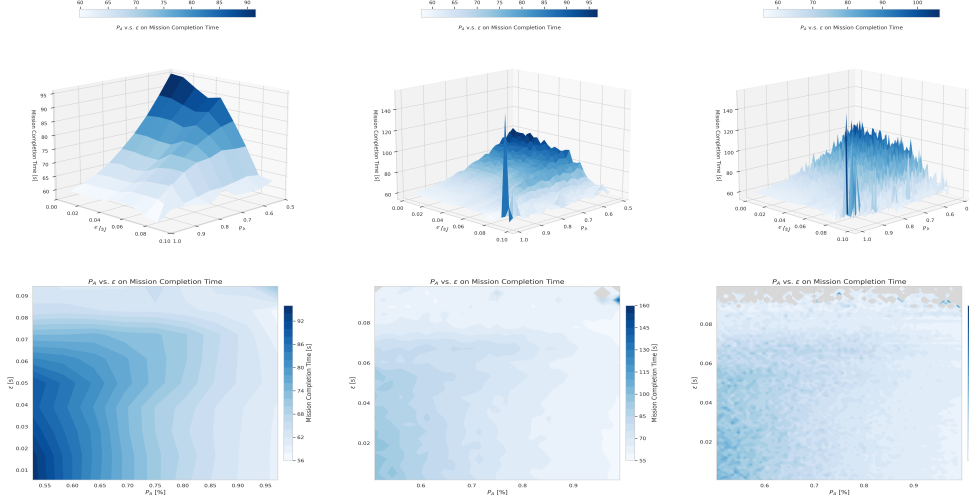


Figure 16: Scenario 2: mission completion time surface (top row) and mission completion time contour (bottom row).

5.3. Analysis of Communicability

As introduced in Section 3.3, communicability as a combined metric to represent RCP key metrics, considers both ε and P_A for a given message transaction time τ_{msg} . τ_{msg} is computed based on the message size (in bits) and the transmission bitrate (in bits per second) as,

$$\tau_{msg} = \frac{S_{bits}}{R_{bitrate}} \quad (72)$$

where τ_{msg} is the message transmission time (seconds), S_{bits} is the size of the message in bits, and $R_{bitrate}$ is the transmission bitrate in bits per second (bps). In this simulation, seven double float control inputs are continuous transmitted between the RPA and RPS, corresponding to a total of $7 \times 8 = 56$ bytes, or,

$$S_{bits} = 56 \text{ bytes} \times 8 \frac{\text{bits}}{\text{byte}} = 448 \text{ bits} \quad (73)$$

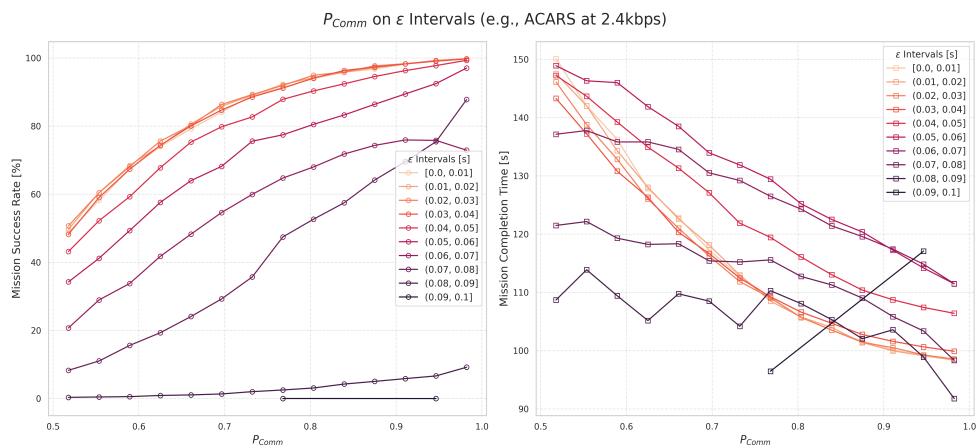
The bitrate is based on the communication infrastructure. We use the Aircraft Communications Addressing and Reporting System (ACARS) in our case study. ACARS is one of the earliest widely adopted digital data link systems in aviation. It enables the secure exchange of short, text-based encrypted messages between aircraft and ground-based operations (i.e., flight

plan updates, weather forecasts) (Roy, 2001; Risley et al., 2001). Traditional VHF ACARS data transmissions use a low data rate around 2.4 kbps (Tooley and Wyatt, 2017). That is,

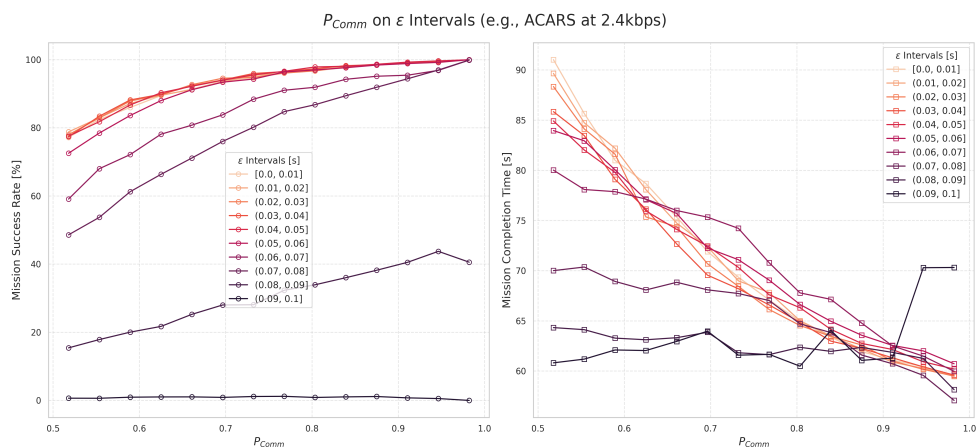
$$R_{bitrate} = 2.4 \times 10^3 \text{ bits/s} \quad (74)$$

and the corresponding message transaction time is,

$$\tau_{msg} = \frac{448 \text{ bits}}{2400 \text{ bits/s}} \approx 0.1867\text{s} \quad (75)$$



(a) Scenario 1.



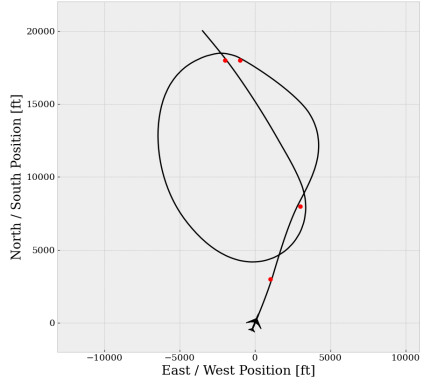
(b) Scenario 2.

Figure 17: Communicability analysis for two waypoint following scenarios. The bitrate is set as 2.4 kbps for VHF ACARS.

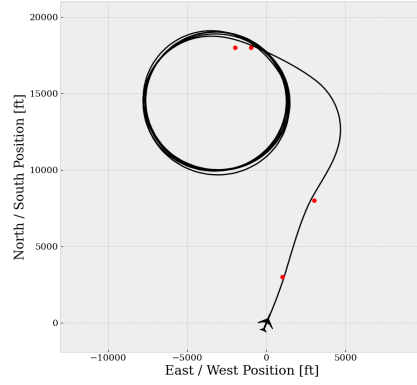
P_{comm} is then calculated with Equation (36). We further draw the mission success rate and mission completion time versus P_{comm} for ε intervals for both scenarios, as in Figure 17. Communicability analysis facilitates better understanding of the maximum tolerable latency value for a given data transmission system. For instance, it is obvious that in Figure 17b, latency of 0.08s still leads to high mission success rate for high communicability in simpler scenarios. Figure 17a also shows the impact of *latency blockage* where a higher latency (i.e., $\varepsilon \in (0.07, 0.08]$) can achieve higher mission success rate than lower latency (i.e., $\varepsilon \in (0.06, 0.07]$), even with high communicability (i.e., $P_{\text{comm}} = 1$). Other aviation communication system (i.e., Ka/Ku-band/L-band SATCOM, Aeronautical Mobile Airport Communication System (AeroMACS)) with different bitrate (i.e., AeroMACS maxed 9.2 Mbps.) can be evaluated in a similar way.

5.4. Investigation on Latency Blockage

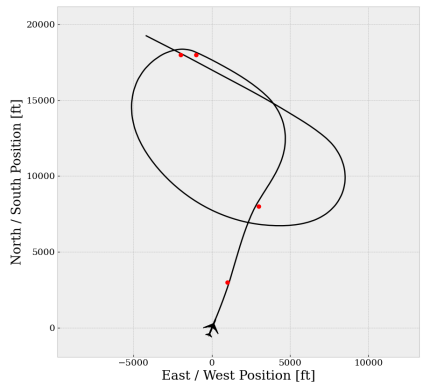
We look further to the *latency blockage* issue highlighted in scenario 1 in this section. Figure 18 provides flight trajectories when $P_A = 1$, and ε ranges from 0.0062s to 0.0067s. In these simulations, no parameter-induced randomness existed due to $P_A = 1$. The simulations in Figure 18a and Figure 18c can complete the task while Figure 18b cannot. The insight is that, in Figure 18b, the flight control is *tricked* into thinking it can reach the last waypoint by conducting minimum radius turns, but if $\varepsilon = 0.062$ or $\varepsilon = 0.064$ the flight control gives up and moves further away to reach the last waypoint. Similar behavior exist for scenarios Figure 18d. This particular behavior is believed to be very scenario and control system dependent due to a latency induced resonance in the minimum radius turn, however, the breakdown of monotonicity with latency may be a general phenomenon that appears in other RPAS missions, scenarios, and control systems.



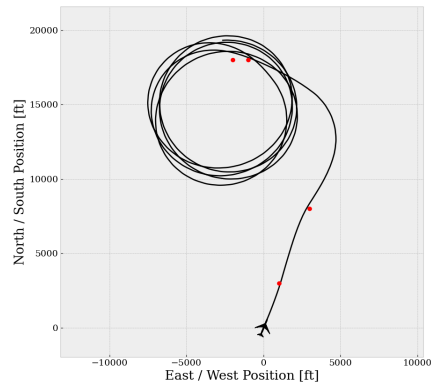
(a) $P_A = 1, \varepsilon = 0.062$.



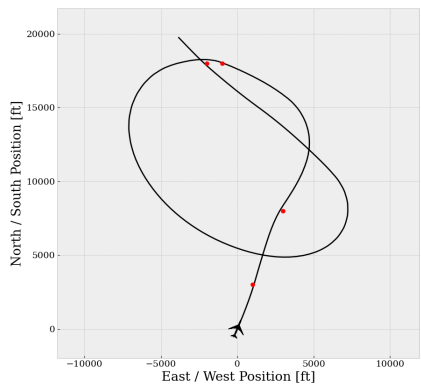
(b) $P_A = 1, \varepsilon = 0.063$.



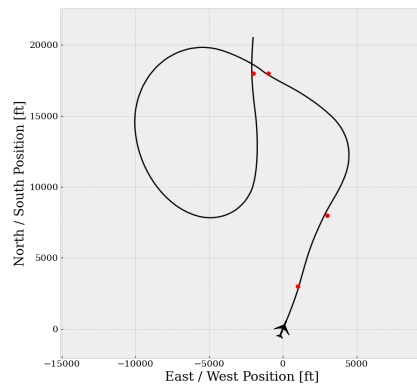
(c) $P_A = 1, \varepsilon = 0.064$.



(d) $P_A = 1, \varepsilon = 0.065$.



(e) $P_A = 1, \varepsilon = 0.066$.



(f) $P_A = 1, \varepsilon = 0.067$.

Figure 18: Flight trajectory in the vertical plane for scenario 1 under different single way latency values ε , showing the communication *latency blockage* for certain ε values for the given task.

6. Conclusions

This study examines how latency and communication availability influence the flight performance of a Remotely Piloted Aircraft System (RPAS), modeled on F-16 dynamics, during a static waypoint-following task. We begin by reviewing relevant aviation communication standards, including ICAO’s Required Communication Performance (RCP) and JARUS’s Required Link Performance (RLP), and then derive their corresponding mathematical formulations. In addition, we propose a new metric, communicability, that collectively represents availability, continuity, and transaction time.

To evaluate flight performance in the context of these communication standards, we define both a complex and a simple scenario, conducting extensive Monte Carlo simulations with randomness from latency and availabilities. These simulations employ key performance measures, such as mission success rate and mission completion time, assessed against varying latency and availability conditions. Finally, we generate a communication reliability surface envelope from the simulation results, offering valuable insights into how communication parameters affect overall RPAS flight performance. We further provide the approach to utilize the communicability concept to help understand the maximum tolerable latency value of assuring mission success and evaluate the flight performance in general. Additionally, we discover the interesting behavior of *latency blockage* to trick the flight control systems into circling, in scenarios with no signal loss at all.

6.1. Limitations

We have several limitations. The experiment was conducted on the simplified open-sourced simulation code of F-16 dynamics, with many assumptions (i.e., without leading edge flaps, approximated aerodynamics coefficients from subsonic flight). A better simulator with broader effective flight envelop makes our study closer to real world scenarios. Moreover, the simulator assume a decoupled flight control on the horizontal and longitudinal planes with two LQRs. Better nonlinear flight control such as NDI exist for F-16 and has been used in the literature. Lastly, we only consider static waypoint reaching task, where a large portion of RPAS usage involves interactions between multiple aircraft in highly dynamic environments.

6.2. Future Studies

The future studies for this work are manifolds,

- Further investigations into more effective optimal control designs are desired. In the current case studies, we consider only the LQR around a single trim point, resulting in suboptimal performance when the state vector operates far from the design setpoint. Gain scheduling at runtime, or control approaches accounting for nonlinear dynamics (e.g., nonlinear dynamics inversion), represent promising directions for future research.
- The current work focuses on static waypoint-following tasks. However, a significant portion of interests lies in flight performance within highly dynamic environments, typically involving multiple moving agents (e.g., collision avoidance, separation violations, tracking). Performance in such dynamic scenarios can be substantially more complex than those examined here.
- As mentioned in Section 5.2.1, Nyquist stability analysis is highly desired to understand and verify phase and gain margins. The open-loop transfer function and the frequency response will need to be derived, especially for Multi-Input Multi-Output (MIMO) systems.
- The experimentation process requires a substantial number of Monte Carlo simulations to produce a high-quality mission success envelope, making real-time estimates of mission completion probabilities impractical. Parallel computing serves as a potential solution (Esselink et al., 1995). Additionally, NVIDIA CUDA enables the agile deployment of thousands of parallel threads, significantly reducing Monte Carlo simulation times at large scales to enable onboard real-time computation.

Acknowledgment

This work was supported by the National Aeronautics and Space Administration (NASA) University Leadership Initiative (ULI) program under project “Autonomous Aerial Cargo Operations at Scale”, via grant No. 80NSSC21M071 to the University of Texas at Austin. The support is gratefully appreciated.

References

Abeyratne, R.I.R., Abeyratne, R.I.R., 2019. Legal priorities in air transport. Springer.

- Ahmad, W., Hasan, O., Pervez, U., Qadir, J., 2017. Reliability modeling and analysis of communication networks. *Journal of Network and Computer Applications* 78, 191–215.
- Alsamhi, S., Ma, O., Ansari, M., 2018. Predictive estimation of the optimal signal strength from unmanned aerial vehicle over internet of things using ann. arXiv preprint arXiv:1805.07614 .
- Asadzadeh, S., de Oliveira, W.J., de Souza Filho, C.R., 2022. Uav-based remote sensing for the petroleum industry and environmental monitoring: State-of-the-art and perspectives. *Journal of Petroleum Science and Engineering* 208, 109633.
- Ashraf, A., Mei, W., Gaoyuan, L., Anjum, Z., Kamal, M.M., 2018. Design linear feedback and lqr controller for lateral flight dynamics of f-16 aircraft, in: 2018 International Conference on Control, Automation and Information Sciences (ICCAIS), IEEE. pp. 367–371.
- Avgousti, S., Panayides, A.S., Christoforou, E.G., Argyrou, A., Jossif, A., Masouras, P., Novales, C., Vieyres, P., 2018. Medical telerobotics and the remote ultrasonography paradigm over 4g wireless networks, in: 2018 IEEE 20th International Conference on e-Health Networking, Applications and Services (Healthcom), IEEE. pp. 1–6.
- Aziz, Z.A., Abdulqader, D.N., Sallow, A.B., Omer, H.K., 2021. Python parallel processing and multiprocessing: A rivew. *Academic Journal of Nawroz University* 10, 345–354.
- Botta, A., Cacace, J., Lippiello, V., Siciliano, B., Ventre, G., et al., 2017. Networking for cloud robotics: A case study based on the sherpa project, in: Proceedings of the International Conference on Cloud and Robotics (ICCR), Saint Quentin, France, pp. 23–23.
- Brehmer, B., 2005. The dynamic ooda loop: Amalgamating boyd’s ooda loop and the cybernetic approach to command and control, in: Proceedings of the 10th international command and control research technology symposium, pp. 365–368.
- Brinker, J.S., Wise, K.A., 1996. Stability and flying qualities robustness of a dynamic inversion aircraft control law. *Journal of Guidance, Control, and Dynamics* 19, 1270–1277.

- Bulusu, V., Chatterji, G.B., Lauderdale, T.A., Sakakeeny, J., Idris, H.R., 2022. Impact of latency and reliability on separation assurance with remotely piloted aircraft in terminal operations, in: AIAA Aviation 2022 Forum, p. 3704.
- Burns, J.O., Mellinkoff, B., Spydell, M., Fong, T., Kring, D.A., Pratt, W.D., Cichan, T., Edwards, C.M., 2019. Science on the lunar surface facilitated by low latency telerobotics from a lunar orbital platform-gateway. *Acta Astronautica* 154, 195–203.
- Byrnes, M.W., 2014. Nightfall machine autonomy in air-to-air combat. *Air & Space Power Journal* 28.
- Chamberlain, R.G., 1966. A space mission success evaluation model. Technical Report.
- Chaturvedi, S.K., Sekhar, R., Banerjee, S., Kamal, H., 2019. Comparative review study of military and civilian unmanned aerial vehicles (uavs). *IN-CAS bulletin* 11, 181–182.
- Chen, J.Y., Haas, E.C., Barnes, M.J., 2007. Human performance issues and user interface design for teleoperated robots. *IEEE Transactions on Systems, Man, and Cybernetics, Part C (Applications and Reviews)* 37, 1231–1245.
- Choi, J.W., Seo, Y.B., 1999. Lqr design with eigenstructure assignment capability [and application to aircraft flight control]. *IEEE Transactions on Aerospace and Electronic Systems* 35, 700–708.
- Dave, G., Choudhary, G., Sihag, V., You, I., Choo, K.K.R., 2022. Cyber security challenges in aviation communication, navigation, and surveillance. *Computers & Security* 112, 102516.
- Dubins, L.E., 1957. On curves of minimal length with a constraint on average curvature, and with prescribed initial and terminal positions and tangents. *American Journal of mathematics* 79, 497–516.
- Esselink, K., Loyens, L., Smit, B., 1995. Parallel monte carlo simulations. *Physical Review E* 51, 1560.

- FAA, 2023. Urban air mobility (uam) concept of operations 2.0). https://www.faa.gov/sites/faa.gov/files/Urban%20Air%20Mobility%20%28UAM%29%20Concept%20of%20Operations%202.0_1.pdf Accessed: 8-6-2024.
- Favre, C., 1994. Fly-by-wire for commercial aircraft: the airbus experience. *International Journal of Control* 59, 139–157.
- Garcia-Perez, C.A., Merino, P., 2016. Enabling low latency services on lte networks, in: 2016 IEEE 1st International Workshops on Foundations and Applications of Self* Systems (FAS* W), IEEE. pp. 248–255.
- Gertler, J., 2012. Us unmanned aerial systems, in: LIBRARY OF CONGRESS WASHINGTON DC CONGRESSIONAL RESEARCH SERVICE.
- Goyal, R., Cohen, A., 2022. Advanced air mobility: Opportunities and challenges deploying evtols for air ambulance service. *Applied Sciences* 12, 1183.
- Guo, W., Brittain, M., Wei, P., 2021. Safety enhancement for deep reinforcement learning in autonomous separation assurance, in: 2021 IEEE International Intelligent Transportation Systems Conference (ITSC), IEEE. pp. 348–354.
- He, S., Lee, C.H., Shin, H.S., Tsourdos, A., 2019. Minimum-effort waypoint-following guidance. *Journal of Guidance, Control, and Dynamics* 42, 1551–1561.
- Heidlauf, P., Collins, A., Bolender, M., Bak, S., 2018. Verification challenges in f-16 ground collision avoidance and other automated maneuvers., in: ARCH@ ADHS, pp. 208–217.
- Hess, R.A., Peng, C., 2018. Design for robust aircraft flight control. *Journal of Aircraft* 55, 875–886.
- Hook, L.R., Clark, M., Sizoo, D., Skoog, M.A., Brady, J., 2016. Certification strategies using run-time safety assurance for part 23 autopilot systems, in: 2016 IEEE Aerospace Conference, IEEE. pp. 1–10.

- Hu, J., Yang, X., Wang, W., Wei, P., Ying, L., Liu, Y., 2020. Uas conflict resolution in continuous action space using deep reinforcement learning, in: AIAA AVIATION 2020 FORUM, p. 2909.
- Hu, J., Yang, X., Wang, W., Wei, P., Ying, L., Liu, Y., 2022. Obstacle avoidance for uas in continuous action space using deep reinforcement learning. *IEEE Access* 10, 90623–90634.
- Huerta, M., 2013. Integration of civil unmanned aircraft systems (uas) in the national airspace system (nas) roadmap. Federal Aviation Administration, Retrieved Dec 19, 2013.
- ICAO, 2006. Icao doc 9869 manual on required communication performance (rcp). https://www.icao.int/safety/acp/repository/9869_en.pdf Accessed: 8-1-2024.
- ICAO ACP-WGF24 WP15, 2011. Unmanned aircraft system - availability, continuity and latency. <https://www.icao.int/safety/acp/ACPWGF/ACP-WG-F-24/ACP-WGF24-WP15%20UAS%20RCP.doc> Accessed: 8-2-2024.
- ICAO AMCP WG-C1/WP8, 2011. Concept of required communication performance (rcp). https://www.icao.int/safety/acp/Inactive%20working%20groups%20library/ACP-WG-C-1/WG1_WP08.doc Accessed: 8-3-2024.
- Iscold, P., Pereira, G.A., Torres, L.A., 2010. Development of a hand-launched small uav for ground reconnaissance. *IEEE Transactions on Aerospace and Electronic Systems* 46, 335–348.
- Jacklin, S.A., 2019. Small-satellite mission failure rates. Technical Report.
- JARUS, R., . Required c2 performance. RLP) concept. JAR_DEL_WG5_D4.
- Jensen, T.M., 2011. Waypoint-following guidance based on feasibility algorithms. Master's thesis. Institutt for teknisk kybernetikk.
- Johnson, W., Silva, C., 2022. Nasa concept vehicles and the engineering of advanced air mobility aircraft. *The Aeronautical Journal* 126, 59–91.

- Kephart, R.J., Braasch, M.S., 2010. See-and-avoid comparison of performance in manned and remotely piloted aircraft. *IEEE Aerospace and Electronic Systems Magazine* 25, 36–42.
- Lee, S., Cho, A., Kee, C., 2010. Integrated waypoint path generation and following of an unmanned aerial vehicle. *Aircraft Engineering and Aerospace Technology* 82, 296–304.
- Lu, Y., Peng, Z., Miller, A.A., Zhao, T., Johnson, C.W., 2015. How reliable is satellite navigation for aviation? checking availability properties with probabilistic verification. *Reliability Engineering & System Safety* 144, 95–116.
- Luck, J.P., McDermott, P.L., Allender, L., Russell, D.C., 2006. An investigation of real world control of robotic assets under communication latency, in: *Proceedings of the 1st ACM SIGCHI/SIGART conference on Human-robot interaction*, pp. 202–209.
- Lupisella, M., Bleacher, J., Lewis, R., Dworkin, J., Wright, M., Burton, A., Rubins, K., Wallace, S., Stahl, S., John, K., et al., 2018. Low-latency telerobotic sample return and biomolecular sequencing for deep space gateway. *LPI Contributions* 2063.
- Markus, P., Eftekari, R., 2020. Existing and emerging communication technologies for upper class e traffic management (etm). *Regulus Group*, March .
- Ma’Sum, M.A., Arrofi, M.K., Jati, G., Arifin, F., Kurniawan, M.N., Mursanto, P., Jatmiko, W., 2013. Simulation of intelligent unmanned aerial vehicle (uav) for military surveillance, in: *2013 international conference on advanced computer science and information systems (ICACISIS)*, IEEE. pp. 161–166.
- Mayer, M., 2015. The new killer drones: Understanding the strategic implications of next-generation unmanned combat aerial vehicles. *International Affairs* 91, 765–780.
- MITRE Engenuity, 2023. Urban air mobility use case uam operations over 5g networks). <https://info.mitre-engenuity.org/hubfs/Open%20Generation/Engenuity%20Urban%20Air%20Mobility%20Use%20Case%20June%202023.pdf> Accessed: 8-6-2024.

- Molnar, T.G., Kannan, S.K., Cunningham, J., Dunlap, K., Hobbs, K.L., Ames, A.D., 2024. Collision avoidance and geofencing for fixed-wing aircraft with control barrier functions. arXiv preprint arXiv:2403.02508 .
- Moore, T., Monteiro, L.S., Hill, C., 2002. Maritime dgps: Ensuring the best availability and continuity. *The Journal of Navigation* 55, 485–494.
- Morelli, E.A., 1998. Global nonlinear parametric modelling with application to f-16 aerodynamics, in: *Proceedings of the 1998 American Control Conference. ACC (IEEE Cat. No. 98CH36207)*, IEEE. pp. 997–1001.
- Muecklich, N., Sikora, I., Paraskevas, A., Padhra, A., 2023. Safety and reliability in aviation—a systematic scoping review of normal accident theory, high-reliability theory, and resilience engineering in aviation. *Safety science* 162, 106097.
- Nguyen, L.T., 1979. Simulator study of stall/post-stall characteristics of a fighter airplane with relaxed longitudinal static stability. volume 12854. National Aeronautics and Space Administration.
- Organization, I.I.C.A., 2017. Remotely piloted aircraft system (rpas) concept of operations for international ifr operations.
- Pachter, M., Kobylarz, T., Houppis, C., 1996. Literal nyquist stability criterion for mimo control systems. *International Journal of Control* 63, 55–65.
- Pang, Y., Zhao, X., Hu, J., Yan, H., Liu, Y., 2022. Bayesian spatio-temporal graph transformer network (b-star) for multi-aircraft trajectory prediction. *Knowledge-Based Systems* 249, 108998.
- Pang, Y., Zhao, X., Yan, H., Liu, Y., 2021. Data-driven trajectory prediction with weather uncertainties: A bayesian deep learning approach. *Transportation Research Part C: Emerging Technologies* 130, 103326.
- Pettit, D., Turnbull, A., Roelant, H.A., 2001. General aviation aircraft reliability study. Technical Report.
- Priyambodo, T.K., Dhewa, O.A., Susanto, T., 2020. Model of linear quadratic regulator (lqr) control system in waypoint flight mission of flying wing uav. *Journal of Telecommunication, Electronic and Computer Engineering (JTEC)* 12, 43–49.

- Reinhardt, D.W., 2013. Safety Assurance of Aviation Systems. Ph.D. thesis. University of York.
- Risley, C., McMath, J., Payne, B., 2001. Experimental encryption of aircraft communications addressing and reporting system (acars) aeronautical operational control (aoc) messages, in: 20th DASC. 20th Digital Avionics Systems Conference (Cat. No. 01CH37219), IEEE. pp. 7D4–1.
- Roy, A., 2001. Secure aircraft communications addressing and reporting system (acars), in: 20th DASC. 20th Digital Avionics Systems Conference (Cat. No. 01CH37219), IEEE. pp. 7A2–1.
- Scherer, J., Yahyanejad, S., Hayat, S., Yanmaz, E., Andre, T., Khan, A., Vukadinovic, V., Bettstetter, C., Hellwagner, H., Rinner, B., 2015. An autonomous multi-uav system for search and rescue, in: Proceedings of the first workshop on micro aerial vehicle networks, systems, and applications for civilian use, pp. 33–38.
- Serafino, G., Derin, D., Babich, F., Pietrosevoli, E., Goiak, M., 2019. Link performance evaluation procedure for the introduction of unmanned air vehicles in civil airspace, in: 2019 IEEE 5th International Workshop on Metrology for AeroSpace (MetroAeroSpace), IEEE. pp. 182–186.
- SESAR-JU, 2019. Sesar joint undertaking, european atm master plan 2020. <https://www.sesarju.eu/masterplan2020> Accessed: 12-12-2024.
- Seto, D., Ferriera, E., Marz, T.F., 1999. Case Study: Development of a Baseline Controller for Automatic Landing of an F-15 Aircraft Using Linear Matrix Inequalities (LMIs). Carnegie Mellon University, Software Engineering Institute.
- Sheridan, T.B., Ferrell, W.R., 1963. Remote manipulative control with transmission delay. *IEEE Transactions on Human Factors in Electronics* , 25–29.
- Sollenberger, R.L., McAnulty, D.M., Kerns, K., et al., 2003. The effect of voice communications latency in high density, communications-intensive airspace. Technical Report. William J. Hughes Technical Center (US).
- Sonneveldt, L., 2006. Nonlinear f-16 model description .

- Stevens, B.L., Lewis, F.L., Johnson, E.N., 2015. Aircraft control and simulation: dynamics, controls design, and autonomous systems. John Wiley & Sons.
- Taylor, J., Makovsky, A., Barbieri, A., Tung, R., Estabrook, P., Thomas, A.G., 2016. Mars exploration rover telecommunications. *Deep Space Communications* , 251–358.
- Teutsch, J., Petersen, I.C., 2022. Communication latency and loss for integrated ifr-rpas movements in the tma, in: 2022 Integrated Communication, Navigation and Surveillance Conference (ICNS), IEEE. pp. 1–18.
- Thammawichai, M., Baliyarasimhuni, S.P., Kerrigan, E.C., Sousa, J.B., 2017. Optimizing communication and computation for multi-uav information gathering applications. *IEEE Transactions on Aerospace and Electronic Systems* 54, 601–615.
- The Performance Based Operations Aviation Rulemaking Committee (PARC), 2018. Satellite voice project report. https://www.faa.gov/sites/faa.gov/files/about/office_org/headquarters_offices/avs/180514_PARCSATVOICEReport.pdf Accessed: 8-2-2024.
- Thirtyacre, D.L., 2021. The effects of remotely piloted aircraft command and control latency during within-visual-range air-to-air combat. Ph.D. thesis. Embry-Riddle Aeronautical University.
- Thirtyacre, D.L., 2022. Remotely piloted aircraft c2 latency during air-to-air combat. *Air & Space Operations Review* 1, 14.
- Tomlin, C., Mitchell, I., Ghosh, R., 2001. Safety verification of conflict resolution manoeuvres. *IEEE Transactions on Intelligent Transportation Systems* 2, 110–120.
- Tooley, M., Wyatt, D., 2017. Aircraft communications and navigation systems. Routledge.
- Trsek, R.B., Maj, U., 2007. The last manned fighter: Replacing manned fighters with ucavs. Air Command and Staff College, Air University .
- Tsurutani, B., Judge, D., Guarnieri, F., Gangopadhyay, P., Jones, A., Nuttall, J., Zambon, G., Didkovsky, L., Mannucci, A., Iijima, B., et al., 2005.

- The october 28, 2003 extreme euv solar flare and resultant extreme ionospheric effects: Comparison to other halloween events and the bastille day event. *Geophysical Research Letters* 32.
- Tsurutani, B., Verkhoglyadova, O., Mannucci, A., Lakhina, G., Li, G., Zank, G., 2009. A brief review of “solar flare effects” on the ionosphere. *Radio Science* 44, 1–14.
- Tsurutani, B.T., Zank, G.P., Sterken, V.J., Shibata, K., Nagai, T., Mannucci, A.J., Malaspina, D.M., Lakhina, G.S., Kanekal, S.G., Hosokawa, K., et al., 2022. Space plasma physics: A review. *IEEE Transactions on Plasma Science* 51, 1595–1655.
- Ukwandu, E., Ben-Farah, M.A., Hindy, H., Bures, M., Atkinson, R., Tachtatzis, C., Andonovic, I., Bellekens, X., 2022. Cyber-security challenges in aviation industry: A review of current and future trends. *Information* 13, 146.
- Villemeur, A., 1992. Reliability, Availability, Maintainability, and Safety Assessment: Assessment, hardware, software, and human factors. volume 2. J. Wiley.
- Voigtländer, F., Ramadan, A., Eichinger, J., Lenz, C., Pensky, D., Knoll, A., 2017. 5g for robotics: Ultra-low latency control of distributed robotic systems, in: 2017 International Symposium on Computer Science and Intelligent Controls (ISCSIC), IEEE. pp. 69–72.
- Vozar, S., Storms, J., Tilbury, D.M., 2018. Development and analysis of an operator steering model for teleoperated mobile robots under constant and variable latencies. *Robotica* 36, 167–186.
- Vozar, S., Tilbury, D.M., 2014. Driver modeling for teleoperation with time delay. *IFAC Proceedings Volumes* 47, 3551–3556.
- Wang, F., Qi, S., Li, J., 2017. An analysis of time-delay for remote piloted vehicle, in: MATEC Web of Conferences, EDP Sciences. p. 04012.
- Weckman, G., Shell, R., Marvel, J., 2001. Modeling the reliability of repairable systems in the aviation industry. *Computers & industrial engineering* 40, 51–63.

- Xue, D., Liu, Z., Zhang, D., Wu, C.L., Yang, J., 2024. Optimizing polar air traffic: Strategies for mitigating the effects of space weather-induced communication failures poleward of 82 n. *Space Weather* 22, e2024SW004136.
- Yang, C.D., Chang, S.Y., 2024. Flight control design based on nonlinear dynamic inversion for post-stall maneuvers .
- Zhao, J., Si, S., Cai, Z., Guo, P., Zhu, W., 2020. Mission success probability optimization for phased-mission systems with repairable component modules. *Reliability Engineering & System Safety* 195, 106750.
- Zhao, Y., Paine, N., Kim, K.S., Sentis, L., 2015. Stability and performance limits of latency-prone distributed feedback controllers. *IEEE Transactions on Industrial Electronics* 62, 7151–7162.